Steric effects in a mean-field model for polar nematic liquid crystals

Fulvio Bisi
Dipartimento di Matematica and CNISM, Università di Pavia, Via Ferrata 1, 27100 Pavia, Italy

André M. Sonnet
Department of Mathematics and Statistics, University of Strathclyde, Livingstone Tower, 26 Richmond Street, Glasgow G1 1XH, Scotland

Epifanio G. Virga
Dipartimento di Matematica and CNISM, Università di Pavia, Via Ferrata 1, 27100 Pavia, Italy

(Received 21 October 2009; revised manuscript received 14 May 2010; published 19 October 2010)

The existence of uniaxial liquid crystals comprising polar molecules, with all the dipoles aligned in a parallel pattern, is classically ruled out. Generally, there are two different avenues to a mean-field theory for liquid crystals: one is based on short-range, repulsive, steric forces, and the other is based on long-range, globally attractive, dispersion forces. Purely polar steric interactions have been shown to have the potential of inducing unexpected orientationally ordered states. In real molecules, anisotropies both in shape and in polarizability coexist; it has been shown that dispersion forces interaction can be combined with hard-core repulsion in a formal theory, based on a *steric tensor*. Starting from this, we build an interaction Hamiltonian featuring the average electric dipolar energy exchanged between molecules with the same excluded region. Under the assumption that the molecular shape is spheroidal, we propose a mean-field model for polar nematic liquid crystals which can exhibit both uniaxial and biaxial polar phases. By means of a numerical bifurcation analysis, we discuss the stability of the equilibrium against the choice of two model parameters, one describing the degree of molecular shape biaxiality and the other describing the relative orientation of the electric dipole within each molecule. We find only uniaxial stable phases, which are effectively characterized by a single scalar order parameter.

DOI: 10.1103/PhysRevE.82.041709 PACS number(s): 61.30.Cz, 61.30.Dk

I. INTRODUCTION

The role played by electric dipolar forces in the structure of classical fluids has long been explored; a fairly complete review can be found in [1,2] (see also [3] for a shorter account on liquid crystals and [4] for one on computer simulations with Gay-Berne mesogens). Though we are here concerned solely with nematic liquid crystals, we broaden our perspective and see how the possible dipolar nature of molecules has been incorporated in other model fluids. In this short account, we shall not follow a historical approach, but we shall rather report a few essential findings, especially relevant to the occurrence of orientationally ordered phases, which form the main subject of our work.

Wei and Patey [5–7] studied by molecular dynamics simulations a fluid of spherical particles interacting through a pair potential that at short distances is isotropically repulsive and at long distances retains the anisotropy induced by point permanent dipoles sitting in the molecules' centers (strongly interacting dipolar *soft* spheres). It was shown that at sufficiently large densities such a fluid undergoes a phase transition, becoming nematic and polar when the density exceeds a critical value. The same scenario was essentially confirmed by computer simulations in [8,9] for dipolar *hard* spheres, which interact through the dipolar pair-potential subject to the constraint that the interacting point dipoles be kept at a distance larger than the molecular diameter. Such a nematic ferroelectric phase was also explored analytically within density functional theory [10] and again numerically under the action of an external electric field [11] which, at sufficiently large densities, induces a transition from a ferroelectric nematic phase to a ferroelectric columnar phase, even for small field strengths.

Further simulation studies on polar hard spheres also performed at low densities [12–14] revealed that no vapor-liquid transition exists when the density is sufficiently low, but instead particles organize themselves in chains where adjacent spheres, which are nearly in contact, have their dipoles in the parallel (head-tail) configuration. Chains are then arranged in such a way that no total dipolar moment is associated with the phases they form, which thus fail to be ferroelectric.

Such a surprising result was also found in [15], where the more general question was asked as to whether dipolar interactions are sufficient to stabilize a liquid phase. In [15] this question was addressed by simulating a system of particles interacting through a pair potential where the dipolar potential was supplemented by the repulsive potential typical of soft spheres (diverging like $1/r^{12}$ for small interparticle distances r) and an attractive potential typical of van der Waals interactions (decaying like $-1/r^6$ for large r). In the computer simulations of [15], the latter attractive potential was balanced against the former repulsive potential by a multiplicative parameter λ; below a certain value of λ no vapor-liquid coexistence could be observed, while particles were seen to arrange themselves in chains with parallel adjacent dipoles. The case where $\lambda=1$ is of special interest, and the corresponding model fluid is named after Stockmayer. The ferroelectricity of this fluid at sufficiently large densities was confirmed within the zero-density approximation to the density functional theory in [16–18].

A vast theoretical literature is devoted to the study of chain formation in dipolar classical fluids; in particular, we

refer the interested reader to the papers [19–22] which employ analytical methods. In these studies, chains of dipolar particles are treated as polymers, in which the individual particles play the role of monomers. It was shown in [21] that ferroelectric ordering in a fluid of chains formed by dipolar hard spheres can indeed occur, but under the assumption that the chains retain their individuality in the ordered phase, an assumption which is not borne out by simulations. On the contrary, as also shown in [21], dipolar hard spheres at sufficiently high density give rise to a ferroelectric phase whose ultimate constituents are the individual spheres, as chains are no longer distinguishable. However, the critical density at which such a transition occurs is at least one order of magnitude lower than that computed by simulation.

Here we are interested in ferroelectric nematic phases, possibly exhibited by elongated molecules bearing a permanent electric dipole. Our digression above into the realm of ferroelectricity arising in condensed phases of dipolar spherical molecules simply shows that ferroelectricity, or phase polarity, which here we regard as its synonym, is not necessarily related to the anisotropy of short-range interactions: as first shown in [5], a ferroelectric phase also arises from dipolar spherical molecules as a result of the anisotropy in the long-range interactions. A criticism of the theories attempting to explain the mechanism underlying the assembling in chains in the low density regime is that they ignore completely any short-range anisotropic correlations (see p. R424 of [1]). If such an omission may already be the main obstacle in the way to a satisfactory theory of polar classical fluids, whose molecules can be treated as being spherical in shape, it is expected to be more so when polar nematic liquid crystals are at issue, as their molecules are elongated in shape. Here the interplay between the anisotropy in long- and short-range interactions is central to the formation of a polar phase.

This is the problem tackled in our paper: to combine the anisotropy of the short-range repulsive interactions and the anisotropy of the long-range dipolar interactions. We explore the occurrence of a polar nematic phase, possibly biaxial, when either the molecular shape is biaxial or the molecular dipole moment is at an angle with the symmetry axis of a uniaxial molecule.

Touching upon the dipolar nature of liquid crystal molecules evokes necessarily the early explanation that was attempted by Born [23,24] for the condensation of a liquid crystal phase. The hypothesis that liquid crystal aggregation would result from dipolar interactions is now known to be incorrect, despite the fact that most liquid crystal molecules possess a permanent dipole moment. Since the seminal works of Onsager [25] and Maier and Saupe [26], it is widely accepted that both anisotropic short-range repulsive forces of a steric nature and anisotropic long-range attractive forces of a dispersive nature can promote the condensation of a nematic phase: the crucial feature both mechanisms have in common is the anisotropy of the molecular shape, which must be sufficiently elongated in one direction for a nematic liquid crystal phase to arise.

For elongated molecules endowed with a permanent dipole moment, the dipolar interaction energy may reveal a varied scenario. For spherical molecules with a point dipole in their centers the dipolar interaction energy U_{dip} is minimized when two spheres touch each other and their dipoles are in the parallel configuration, whereas U_{dip} only attains a relative minimum when the dipoles of the interacting spheres in contact are in the antiparallel configuration. For elongated molecules the dependence of U_{dip} on the distance between the point dipoles, which is immaterial for spherical molecules, may be responsible for making U_{dip} attain its minimum in the antiparallel configuration, with both dipole moments orthogonal to the line joining the point dipoles, provided in this configuration the point dipoles can approach one another at a smaller distance than in the parallel configuration with both dipole moments parallel to the line joining the point dipoles.

A vast literature is devoted to the effect of adding a dipole moment to the model molecules of a nematic phase; we are especially interested in the contributions concerned with the possibility that such an addition results in making the nematic phase ferroelectric. Nematic molecules were treated as hard axisymmetric ellipsoids in [27], for which it was shown that an additional dipole moment aligned with the molecule's symmetry axis may affect the transition temperature, mostly reducing it, but it is not capable of inducing any macroscopic polarity, a conclusion also confirmed in [28]. A consistent molecular theory to explain the effect on the nematic-to-isotropic transition temperature of a central longitudinal dipole embedded in elongated molecules subject to the classical Maier-Saupe interaction was proposed in [29], which showed how dimerization of molecules with dipoles in the antiparallel configuration can also reduce the nematic-to-isotropic transition temperature upon increasing the strength of the molecular dipole moment. As shown in [30], moving a point dipole along the symmetry axis of a hard spherocylinder, so as to bring it away from the molecular center of inversion, while keeping the dipole moment parallel to the symmetry axis, may destabilize the nematic phase, possibly determining a reentrant isotropic phase, but again it cannot induce ferroelectricity.

Polar nematic phases were instead predicted in [31,32] for both ellipsoids of revolution and spherocylinders endowed with a dipole moment along the molecular axis of symmetry. These studies are based on the density functional theory that attempts to treat more accurately the long-range dipolar interaction; this might explain the different prediction on the existence of a polar nematic phase obtained there. An independent confirmation of this state of affairs came from [33], where a system of hard spherocylinders endowed with a permanent point dipole with dipole moment along the particle's symmetry axis is treated within the Onsager formalism: besides the usual nonpolar nematic phase, a polar nematic phase is formed, into which the isotropic phase can also condense directly.

More general models have also been proposed, in which an effective pair potential is posited that does not derive from a specific molecular model, but possesses instead the symmetry properties common to all interactions compatible with a polar molecular interaction. Such an effective pair potential is treated through different methods: a classical mean-field theory in [34,35] (see also [36] for an extension to a nonextensive statistics), and a two-site cluster method in [37]. The advantage with such a general approach is that the molecular

mechanism behind the polar component of the interaction need not be specified, and could in principle even be unrelated to dipole-dipole interactions; the disadvantage lies correspondingly in the difficulty to relate the parameters of the general pair potential to the characteristics of a specific molecule.

Subtle arguments were employed in [34] to establish the sign of parameters in the expression posited for the pair potential, starting from some properties of the molecules, including the ability to interact through their permanent dipoles. As a result of such a molecular characterization, the mean-field analysis of [34] established that a ferroelectric nematic phase is favored for *oblate*, disklike molecules, that is, for molecules with a dipole moment orthogonal to the direction along which they are elongated.

When molecules are elongated in one direction, but their shape is not invariant under central inversion, that is, when molecules exhibit a *shape polarity*, this latter may interfere with the molecular electric dipole, and possibly even contrast the growth of a ferroelectric phase. It has indeed been shown [38] that molecular shape dipoles tend to orient themselves in the antiparallel configuration if the mutual excluded volume is to be minimized (see also [34] for some anticipating remarks to this effect). Whether electric dipoles would exhibit the same tendency or not should result from a subtle interplay between the relative orientation of shape and electric dipoles in an individual molecule and the details of the molecular shape. Explaining this interplay is indeed the main purpose of our present endeavor, which we start to present in this paper.

Allowing for the shape and electric dipoles to differ in orientation within a single molecule or, more simply, allowing the electric dipole to be oriented differently than the molecule's symmetry axis, brings in naturally the question whether the condensed nematic phase could also be biaxial, besides being ferroelectric. Simulations with disklike molecules endowed with a transverse electric dipole [39] have ruled out phase biaxiality, though local biaxial order was indeed found. More recently, experimental evidence for a biaxial ferroelectric phase has been provided through second harmonic generation measures on a commercially available polymer (Vectra) capable of forming nematic liquid crystals [40]. This polymer exhibits a permanent electric dipole skew to the direction of the main molecular chain.

We pursue our program by combining in a mean-field model both steric short-range repulsive forces which reflect the molecular shape, possibly including its polarity, and long-range attractive forces, prevailingly due to the interaction of permanent electric dipoles. Following the ideas discussed in [41] to describe the average steric alterations of dispersion forces interactions, we introduce a *steric tensor* appropriate to account for molecular hindrance within the mean-field approximation. The definition of this tensor and its role in arriving at an effective interaction Hamiltonian suitable to a mean-field treatment are presented in Sec. II. In Sec. III, we describe the general class of molecular shapes for which we are able to compute analytically the steric tensor for dipolar interactions: these are biaxial spheroids, perturbations of a sphere for which the shape dipole vanishes at the degree of approximation we can handle analytically. Though lacking shape polarity, the molecules we consider exhibit two independent sources of biaxiality: one coming from their shape, the other coming from the arbitrary orientation of the electric dipole relative to the molecular symmetry axes. In Sec. IV, we illustrate the analysis of the mean-field free energy stemming from the effective Hamiltonian described in Sec. III. Since the Hamiltonian is *partly repulsive*, as are many in Straley's general family for nonpolar biaxial nematic liquid crystals [42,43], we resort to a minimax principle that characterizes all phases that can compete for the best mean-field equilibrium [44]. The condensed phases and their polarity are found, for varying temperature, through a bifurcation analysis. We eventually find polar phases, but these fail to be biaxial. In Sec. V, we summarize the conclusions of our study and we comment upon the issues it could not resolve. Finally, the paper is closed by three appendices with several mathematical details of our analysis.

II. STERIC TENSOR FOR DIPOLAR INTERACTIONS

In this section, we construct the pair potential on which we shall build in Sec. IV our mean-field analysis. We ideally decompose the interaction between dipolar molecules in a long-range component and a short-range component. We assume that the former component is dominated by the interaction between permanent molecular dipole moments, while the latter component is mainly of a steric nature. Both these components are separately described below.

A. Dipolar interaction

Consider two electric point dipoles with dipole moments $\boldsymbol{p}$ and $\boldsymbol{p}'$, occupying the positions p_0 and p_0' in space. Their interaction energy U_{dip} can be written as

$$U_{\mathrm{dip}} = \frac{1}{4\pi\epsilon_0 r^3}\{\boldsymbol{p}\cdot\boldsymbol{p}' - 3(\boldsymbol{p}\cdot\boldsymbol{e}_r)(\boldsymbol{p}'\cdot\boldsymbol{e}_r)\}$$

$$= \frac{1}{4\pi\epsilon_0 r^3}\boldsymbol{p}\cdot(\mathbf{I} - 3\boldsymbol{e}_r\otimes\boldsymbol{e}_r)\boldsymbol{p}', \tag{1}$$

where ϵ_0 is the dielectric constant in vacuum, $\mathbf{I}$ is the identity tensor, r is the distance between p_0 and p_0', and $\boldsymbol{e}_r$ is the unit vector along the straight line joining these points; in formulas,

$$r := |p_0' - p_0| \quad \text{and} \quad \boldsymbol{e}_r := \frac{1}{r}(p_0' - p_0). \tag{2}$$

It is easily seen that, for given p_0 and p_0', U_{dip} attains its absolute minimum in the parallel configuration, that is, for $\boldsymbol{p}=\boldsymbol{p}'$ and $\boldsymbol{p}\|\boldsymbol{e}_r$, while U_{dip} attains a local minimum in the antiparallel configuration, that is, for $\boldsymbol{p}'=-\boldsymbol{p}$ and $\boldsymbol{p}\perp\boldsymbol{e}_r$.

B. Effective pair potential

U_{dip} is a potential energy of *soft forces*. For polar molecules, it is the first term in a multipole expansion, valid only if p_0 and p_0' are sufficiently far apart. These long-range forces are complemented by short-range, *hard forces* which represent the steric hindrance to molecular interactions. While di-

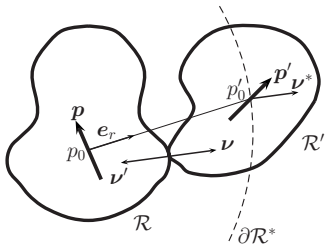

FIG. 1. The van der Waals regions $\mathcal{R}$ and $\mathcal{R}'$ surrounding the point dipoles $\boldsymbol{p}$ and $\boldsymbol{p}'$ placed at positions p_0 and p_0' in space. The unit vector $\boldsymbol{e}_r$ is directed from p_0 to p_0'; $\boldsymbol{\nu}$ and $\boldsymbol{\nu}'$ are the unit outer normals to $\mathcal{R}$ and $\mathcal{R}'$, respectively. The boundary $\partial\mathcal{R}^*$ of the excluded region $\mathcal{R}^*$ is the set of all points that p_0' can reach while $\partial\mathcal{R}'$ glides without rolling over $\partial\mathcal{R}$. The unit vector $\boldsymbol{\nu}^*$ is the outer normal to $\partial\mathcal{R}^*$.

polar forces are attractive, as are most long-range forces, hard steric forces are repulsive. We imagine a simple picture to describe these latter: we think of the points p_0 and p_0' as surrounded by three-dimensional regions, $\mathcal{R}$ and $\mathcal{R}'$, respectively, which represent the ranges of the repulsive hard forces. These essentially make $\mathcal{R}$ and $\mathcal{R}'$ impenetrable to one another, while they lie dormant whenever $\mathcal{R}$ and $\mathcal{R}'$ are not in contact. $\mathcal{R}$ and $\mathcal{R}'$, which we call the van der Waals regions for the two interacting molecules, reflect the molecular shapes, though they need not coincide with them.

Molecular interactions are ultimately responsible for the mesogenic behavior of some molecules which, unlike others, tend to form ordered phases. Often, a theoretical understanding of these ordering transitions is achieved within the mean-field approximation, as in the celebrated Maier-Saupe theory [26]. Replacing a space-dependent energy like U_{dip} with a space-independent one is crucial to the success of any such theory [45]. This is achieved by assuming that molecules sharing one and the same relative orientation are isotropically distributed in space around any given probe molecule and by computing an effective interaction energy between the probe and all other molecules, which are assumed to be immersed in a vacuum.

The interaction energy [Eq. (1)] depends via $\boldsymbol{e}_r$ on the relative position of the two molecules and via $\boldsymbol{p}$ and $\boldsymbol{p}'$ on their relative orientation. The relative hindrance of the van der Waals regions introduces in the effective intermolecular forces a dependence upon the relative molecular orientation subtler than the one explicitly appearing in Eq. (1). Following [41], we now make this idea more precise. As shown in Fig. 1, for given $\mathcal{R}$ and $\mathcal{R}'$, there is a region $\mathcal{R}^*$ in space, depending on $\mathcal{R}$ and $\mathcal{R}'$, inaccessible to the point dipole in p_0' if $\mathcal{R}$ and $\mathcal{R}'$ are mutually impenetrable. We call $\mathcal{R}^*$ the *excluded region*. As suggested by Fig. 1, the boundary $\partial\mathcal{R}^*$ of the excluded region is traced by p_0' while $\partial\mathcal{R}'$ glides without rolling over $\partial\mathcal{R}$. Similarly, the region inaccessible to p_0 by the impenetrability of $\mathcal{R}'$ is traced by all possible trajectories described by p_0 while $\partial\mathcal{R}$ glides without rolling over $\partial\mathcal{R}'$. Since in both cases the relative motion between $\mathcal{R}$ and $\mathcal{R}'$, regarded as rigid bodies, is purely translational, the excluded regions obtained in these two ways simply differ by a translation.

We are not concerned here with smectic phases, and so no positional order will possibly be conceived to arise among molecules. The molecular distribution in space will be taken to be homogeneous. This allows us to define the effective *dipolar pair potential* H_{dip} as the average dipolar energy exchanged between two molecules with a given relative orientation, while their relative position varies freely in space. Any two such molecules share the same excluded region $\mathcal{R}^*$. To account effectively for the presence of more than a pair of molecules in the system, we imagine that an infinite number of molecules, all equally oriented, are uniformly distributed in space so that the same number of molecules, N_{mac}, would be present in the same macroscopic volume V_{mac}. Let a probe molecule wander about the molecules of this system, while keeping its orientation unchanged. For any given molecule in the system, the total energy exchanged with the probe molecule can be computed by imagining this latter exploring an influence ball $\mathbb{B}_{\mathrm{i}}$ with radius R_{i} around the given molecule and then taking the limit as $R_{\mathrm{i}} \to \infty$. Repeating this argument for each molecule in the system reproduces the same result, given the homogeneity of the molecular distribution, and so the average energy is finally estimated by multiplying the total energy exchanged between a single molecule and its probe companion by the number density $\varrho := N_{\mathrm{mac}}/V_{\mathrm{mac}}$.

Such an averaging, typical of mean-field treatments, is bound to remove from our model the collective behaviors characteristic of long-range dipolar interactions, such as the dependence of the phase diagrams upon the shape of the sample for ferroelectric dipolar fluids [16] and the equilibrium spatially nonuniform, orientationally ordered structures, including the vortices and domain walls predicted in [46,47].

Making precise the above definition for H_{dip}, we obtain from Eq. (1) that

$$H_{\mathrm{dip}} := \frac{\varrho}{4\pi\epsilon_0}\boldsymbol{p}\cdot\left[\lim_{R_{\mathrm{i}}\to\infty}\int_{\mathbb{B}_{\mathrm{i}}\setminus\mathcal{R}^*}\frac{1}{r^3}(\mathbf{I}-3\boldsymbol{e}_r\otimes\boldsymbol{e}_r)dV\right]\boldsymbol{p}', \quad (3)$$

where V is the volume measure in the three-dimensional Euclidean space $\mathcal{E}$. Differently said, Eq. (3) can be obtained from integrating over all admissible space the interaction in Eq. (1) multiplied by the probability of finding an interacting molecule at any given point in space, that is, the number density ϱ.

In principle, $\mathcal{R}^*$ can be defined for two arbitrary regions $\mathcal{R}$ and $\mathcal{R}'$, as in Fig. 1. However, in our case the two interacting molecules are identical so that $\mathcal{R}$ and $\mathcal{R}'$ differ only by a rigid rotation $\mathbf{R}$, as do correspondingly $\boldsymbol{p}$ and $\boldsymbol{p}' = \mathbf{R}\boldsymbol{p}$. Thus, H_{dip} ultimately depends on $\mathbf{R}$: explicitly through $\boldsymbol{p}'$, and implicitly through $\mathcal{R}^*$.

C. Steric tensor

Normally, the excluded region $\mathcal{R}^*$ will be *star-shaped*, that is, it can be represented as

$$\mathcal{R}^* = \{p_0' \in \mathcal{E} : |p_0' - p_0| < u^*(\boldsymbol{e}_r)\}. \quad (4)$$

Here the *shape function* u^* is defined in such a way that the mapping $\boldsymbol{e}_r \mapsto u^*(\boldsymbol{e}_r)\boldsymbol{e}_r$ maps the unit sphere $\mathbb{S}^2$ around p_0 into $\partial\mathcal{R}^*$. In this case, the radial integration in Eq. (3) can be performed explicitly, and one finds that

$$H_{\mathrm{dip}} = \frac{\varrho}{4\pi\epsilon_0} \lim_{R_{\mathrm{i}}\to\infty} \int_{\mathbb{S}^2} dA(\boldsymbol{e}_r) \int_{u^*(\boldsymbol{e}_r)}^{R_{\mathrm{i}}} \frac{1}{r} \boldsymbol{p}\cdot(\mathbf{I}-3\boldsymbol{e}_r\otimes\boldsymbol{e}_r)\boldsymbol{p}'\,dr$$

$$= \frac{\varrho}{\epsilon_0} \boldsymbol{p}\cdot\mathbf{S}_{\mathcal{R}^*}\boldsymbol{p}', \tag{5}$$

where $\mathbb{S}^2$ is the unit sphere and A the area measure over it. In Eq. (5) we have introduced the second-rank tensor $\mathbf{S}_{\mathcal{R}^*}$ defined as

$$\mathbf{S}_{\mathcal{R}^*} := \lim_{R_{\mathrm{i}}\to\infty} \fint_{\mathbb{S}^2} \ln\left(\frac{R_{\mathrm{i}}}{u^*(\boldsymbol{e}_r)}\right)(\mathbf{I}-3\boldsymbol{e}_r\otimes\boldsymbol{e}_r)dA(\boldsymbol{e}_r), \tag{6}$$

where $\fint_{\mathbb{S}^2} dA := \frac{1}{4\pi}\int_{\mathbb{S}^2} dA$ denotes the average over $\mathbb{S}^2$. We call $\mathbf{S}_{\mathcal{R}^*}$ the *steric tensor* because it depends only on the shape of the excluded region and can in principle be computed once $u^*(\boldsymbol{e}_r)$ is known.

A simple mathematical property of $\mathbf{S}_{\mathcal{R}^*}$ is worth noting, as it simplifies computing the limit in Eq. (6) and it has an interesting physical consequence. Since, as can easily be shown (see, for example, Appendix A of [41]),

$$\fint_{\mathbb{S}^2} (\mathbf{I}-3\boldsymbol{e}_r\otimes\boldsymbol{e}_r)dA(\boldsymbol{e}_r) = \mathbf{0}, \tag{7}$$

it follows from Eq. (4) that $\mathbf{S}_{\mathcal{R}^*}$ is invariant under rescaling of $\mathcal{R}^*$: changing the shape function u^* into μu^*, for any $\mu > 0$, leaves $\mathbf{S}_{\mathcal{R}^*}$ unchanged. In particular, the integral in the definition of $\mathbf{S}_{\mathcal{R}^*}$ is thus also independent of R_{i}, and the limit trivial. For convenience, we hereafter replace R_{i} in Eq. (6) by the average molecular radius R, which yields

$$\mathbf{S}_{\mathcal{R}^*} = \fint_{\mathbb{S}^2} \ln\left(\frac{R}{u^*(\boldsymbol{e}_r)}\right)(\mathbf{I}-3\boldsymbol{e}_r\otimes\boldsymbol{e}_r)dA(\boldsymbol{e}_r). \tag{8}$$

Put differently, the inner integral in Eq. (5) taken over any spherical shell of inner radius $R_u \geq \max_{\mathbb{S}^2}(u^*)$ vanishes. All contributions to H_{dip} then come from the inner boundary of the integral, $\partial\mathcal{R}^*$: we could indeed rephrase Eq. (5) as

$$H_{\mathrm{dip}} = \frac{\varrho}{4\pi\epsilon_0} \int_{\mathbb{S}^2} dA(\boldsymbol{e}_r) \int_{u^*(\boldsymbol{e}_r)}^{\max_{\mathbb{S}^2}(u^*)} \frac{1}{r} \boldsymbol{p}\cdot(\mathbf{I}-3\boldsymbol{e}_r\otimes\boldsymbol{e}_r)\boldsymbol{p}'\,dr. \tag{9}$$

If $\mathcal{R}$ and $\mathcal{R}'$ are both spheres with radius R, then $\mathcal{R}^*$ is a sphere of radius $2R$, and so, again by Eq. (7), $\mathbf{S}_{\mathcal{R}^*}$ vanishes and $H_{\mathrm{dip}} \equiv 0$. This shows that, for homogeneous assemblies of spherical molecules where the intermolecular vector is isotropically distributed in space, dipolar interactions would be completely masked by steric hindrance. In general, for nonspherical molecular shapes, $\mathbf{S}_{\mathcal{R}^*}$ does not vanish, and a residual dipolar interaction survives in H_{dip}, determined essentially by the short-range behavior of U_{dip}. The long-range dependence of U_{dip} is washed away by our assuming that the influence region $\mathbb{B}_{\mathrm{i}}$ has a spherical shape.[1] Effectively, such an assumption makes our interaction U_{dip} equivalent to a short-range dipolar interaction, though it was long range to start with. Actually, it is remarkable that our spherical symmetry assumption lets any anisotropic interaction survive in H_{dip}, albeit short range. Such a conclusion is also in agreement with Groh and Dietrich's treatment [17] of the dependence on sample's shape of the effective interaction potential for Stockmayer fluids in a vacuum: for a spherical sample's shape, that is, for $k=1$ in Eq. (3.20) of [17], the effective interaction potential vanishes identically. Whereas in Groh and Dietrich's approach molecules are spherical and sample's shapes are ellipsoidal, in ours, molecules are ellipsoidal and the sample's shape is spherical: in the only case where these two approaches can be compared, they agree.

III. BIAXIAL SPHEROIDAL MOLECULES

To compute analytically $\mathbf{S}_{\mathcal{R}^*}$, we employ, as in [41], a specific family of molecular shapes, which is described below. For the shapes in this family we then obtain explicitly H_{dip} from Eq. (5) and we explore its properties.

A. Spheroidal shape

We adopt a perturbation approach and we assume that $\partial\mathcal{R}$ is nearly a sphere of radius R. More precisely, we assume that $\partial\mathcal{R}$ is the image under the mapping $\boldsymbol{e}_r \mapsto u_r(\boldsymbol{e}_r)\boldsymbol{e}_r$, with

$$u(\boldsymbol{e}_r) = R[1+\varepsilon u_r(\boldsymbol{e}_r)], \tag{10}$$

of the unit sphere $\mathbb{S}^2$ around p_0. In Eq. (10), ε is a perturbation parameter and u_r is subject to

$$\fint_{\mathbb{S}^2} u_r(\boldsymbol{e}_r)d\boldsymbol{A}(\boldsymbol{e}_r) = 0, \tag{11}$$

which allows us to interpret R as the average molecular radius.

For the quasispherical particles described by Eq. (10), one might expect that the isotropic-to-nematic transition could only take place at unrealistic temperatures or densities; similarly, one might suspect that the influence on that transition of the dipolar nature of the fluid can only be effective for dipolar moments so large to make our mean-field treatment inapplicable, but, as will be clear shortly below, the major merit of our approach is that it is analytic and explicit, and we believe that it is indicative of what happens for more realistic molecular shapes.

As shown in [41], to within first order in ε, $\partial\mathcal{R}^*$ can be represented as the image of the unit sphere $\mathbb{S}^2$ around p_0 through the mapping $\boldsymbol{e}_r \mapsto u^*(\boldsymbol{e}_r)\boldsymbol{e}_r$, with

[1] This is not the case for quadrupolar interactions, for which the law of decay in the integrand of Eq. (5) is stronger than $1/r$, and so the long-range tail of the interaction does not contribute to the effective Hamiltonian, irrespective of the shape of the influence region [41].

$$u^*(\boldsymbol{e}_r) = 2R\left\{1 + \varepsilon\frac{1}{2}[u_r(\boldsymbol{e}_r) + u_r(-\mathbf{R}^{\mathsf{T}}\boldsymbol{e}_r)]\right\} + o(\varepsilon), \quad (12)$$

where $\mathbf{R}$ is the rotation by which $\mathcal{R}'$ differs from $\mathcal{R}$. Within our shape approximation [Eq. (10)], the function in Eq. (12) represents the distance of *closest approach* between two molecules, which plays a central role in colloid science. As also witnessed by some recent work [48,49], mostly related to liquid crystals, determining this function is not in general an easy task, despite its deceivingly simple, direct geometric definition. Formula (12) owes its simplicity to the spheroidal approximation adopted here.

By Eqs. (7) and (11), we can write the steric tensor in Eq. (6) as

$$\mathbf{S}_{\mathcal{R}^*} = \frac{3}{2}\varepsilon\oint_{\mathbb{S}^2}[u_r(\boldsymbol{e}_r) + u_r(-\mathbf{R}^{\mathsf{T}}\boldsymbol{e}_r)]\boldsymbol{e}_r \otimes \boldsymbol{e}_r dA(\boldsymbol{e}_r) + o(\varepsilon). \quad (13)$$

We now assume a quadrupolar shape for $\mathcal{R}$, that is, we represent u_r through the *shape tensor* $\mathbf{E}$,

$$u_r(\boldsymbol{e}_r) = \boldsymbol{e}_r \cdot \mathbf{E}\boldsymbol{e}_r, \quad (14)$$

where $\mathbf{E}$ satisfies the conditions

$$\mathbf{E} = \mathbf{E}^{\mathsf{T}} \quad \text{and} \quad \operatorname{tr}\mathbf{E} = 0, \quad (15)$$

which, again by Eq. (7), make Eq. (11) valid. By inserting Eq. (14) into Eq. (12) and making use of the identity (see, for example, Appendix A of [41])

$$\oint_{\mathbb{S}^2} e_i e_j e_k e_l dA(\boldsymbol{e}_r) = \frac{1}{15}(\delta_{ij}\delta_{kl} + \delta_{ik}\delta_{jl} + \delta_{il}\delta_{jk}),$$

where e_i are the Cartesian components of $\boldsymbol{e}_r$, one easily checks that within the family of molecular shapes under consideration the steric tensor can be written as

$$\mathbf{S}_{\mathcal{R}^*} = \frac{\varepsilon}{5}(\mathbf{E} + \mathbf{E}') + o(\varepsilon), \quad (16)$$

where

$$\mathbf{E}' := \mathbf{R}\mathbf{E}\mathbf{R}^{\mathsf{T}} \quad (17)$$

is the shape tensor for $\mathcal{R}'$. As a result, the dipolar pair potential in Eq. (5) takes the form

$$H_{\mathrm{dip}} = \frac{\varepsilon\varrho}{5\epsilon_0}\boldsymbol{p}\cdot(\mathbf{E} + \mathbf{E}')\boldsymbol{p}' + o(\varepsilon). \quad (18)$$

We shall write $\boldsymbol{p} = p\boldsymbol{\ell}$, where p is the scalar electric dipole moment of each molecule, so that the unit vector $\boldsymbol{\ell} \in \mathbb{S}^2$ along the permanent electric molecular dipole describes the *molecular electric polarity*. If we neglect higher order terms in ε, H_{dip} in Eq. (18) thus becomes

$$H_{\mathrm{dip}} = U_0(\mathbf{E}\boldsymbol{\ell}\cdot\boldsymbol{\ell}' + \mathbf{E}'\boldsymbol{\ell}'\cdot\boldsymbol{\ell}), \quad (19)$$

where $\boldsymbol{\ell}' := \mathbf{R}\boldsymbol{\ell}$, and $U_0 := \varepsilon\varrho p^2/5\epsilon_0$ expresses the strength of the interaction.

Furthermore, we assume that the shape tensor in Eq. (14) has the general biaxial form

$$\mathbf{E} = \mathbf{q} + \lambda\mathbf{b}, \quad (20)$$

where

$$\mathbf{q} := \boldsymbol{m}\otimes\boldsymbol{m} - \frac{1}{3}\mathbf{I}, \quad (21a)$$

$$\mathbf{b} := \boldsymbol{e}\otimes\boldsymbol{e} - \boldsymbol{e}_\perp\otimes\boldsymbol{e}_\perp \quad (21b)$$

are the traceless molecular tensors introduced in [50] and adopted to describe the general quadrupolar interaction of molecules endowed with D_{2h} symmetry along the axes $(\boldsymbol{e},\boldsymbol{e}_\perp,\boldsymbol{m})$ [42,43,51–53]. The unit vector $\boldsymbol{m}$ in Eq. (21a) represents the long molecular axis, that is, the axis along which the molecule is elongated. Thus, the eigenvalue of $\mathbf{E}$ relative to $\boldsymbol{m}$ must be the largest eigenvalue of $\mathbf{E}$, and so positive, by Eq. (15). As is easily seen, this requires λ to be in the interval $[-1,1]$. For $\lambda=-1$, the shape tensor $\mathbf{E}$ describes a disklike molecule symmetric about $\boldsymbol{e}$, whereas, for $\lambda=1$, $\mathbf{E}$ describes a disklike molecule symmetric about $\boldsymbol{e}_\perp$. For both $\lambda=\pm\frac{1}{3}$, $\mathbf{E}$ exhibits the largest biaxiality as $\det\mathbf{E}=0$: either the eigenvalue relative to $\boldsymbol{e}$ or the one relative to $\boldsymbol{e}_\perp$ vanishes. For $\lambda=0$, the molecule has a uniaxial shape, symmetric about $\boldsymbol{m}$. For any other value of λ the molecular shape is an ellipsoid with axes along the frame $(\boldsymbol{e},\boldsymbol{e}_\perp,\boldsymbol{m})$ (see Fig. 2).

In general, the dipole moment need not be directed along $\boldsymbol{m}$. Another model parameter is the angle α between the unit vectors $\boldsymbol{m}$ and $\boldsymbol{\ell}$. Here we choose to place the unit vectors $\boldsymbol{e}$, $\boldsymbol{\ell}$, and $\boldsymbol{m}$ all in the same plane, so as to represent the molecular electric polarity as

$$\boldsymbol{\ell} = \cos\alpha\boldsymbol{m} + \sin\alpha\boldsymbol{e}, \quad (22)$$

thus designating the plane $(\boldsymbol{m},\boldsymbol{e})$ as the one where both the molecular shape elongation and the molecular electric polarity lie. Without loss of generality, we can assume that $\alpha \in [0,\frac{\pi}{2}]$.

B. Ground state

Direct inspection of Eq. (1) shows that the antiparallel configuration, in which $\boldsymbol{p}'=-\boldsymbol{p}$ and $\boldsymbol{p}\perp\boldsymbol{e}_r$, can indeed become the absolute minimizer for U_{dip} whenever the distance $r_\perp$ of closest approach in this configuration and the distance $r_\parallel$ of closest approach in the parallel configuration, for which $\boldsymbol{p}=\boldsymbol{p}'$ and $\boldsymbol{p}\parallel\boldsymbol{e}_r$, are such that $r_\parallel/r_\perp > \sqrt[3]{2}$. Since, according to Eq. (12), this ratio is close to unity in our linear approximation, the absolute minimizer of U_{dip} remains the parallel configuration $\boldsymbol{\ell}=\boldsymbol{\ell}'$, but, as shown in Appendix A, it is staggered, that is, with the intermolecular vector neither parallel nor orthogonal to $\boldsymbol{\ell}$. The configuration that minimizes the effective, purely orientational pair potential H_{dip} may differ from the parallel configuration as a result of a collective average behavior which is not intuitively justifiable only in terms of the absolute minimizer of U_{dip}. We shall determine below how the ground state of H_{dip} depends on the model parameters (λ,α) chosen in the parameter space $\mathcal{P}$ depicted in Fig. 3.

By inserting both Eqs. (22) and (20) into Eq. (19), we arrive at the following explicit representation for H_{dip}:

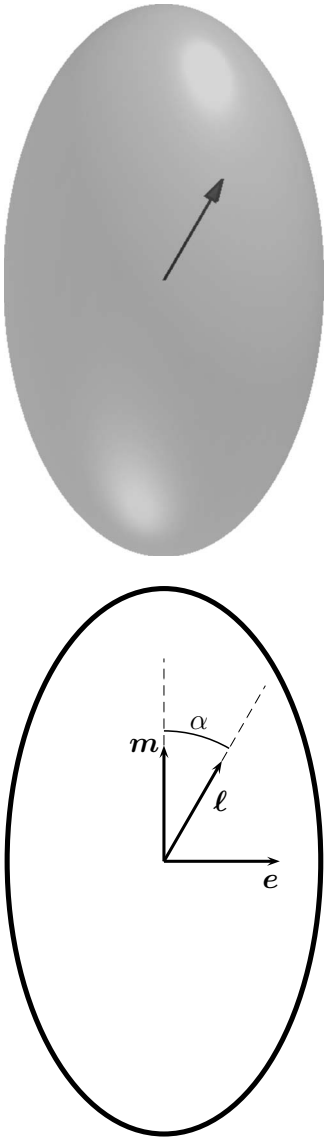

FIG. 2. Cartoon of the ellipsoid describing the molecular shape. The unit vector $\boldsymbol{\ell}$ describes the molecular electric polarity; $\boldsymbol{m}$ and $\boldsymbol{e}$ are the unit vectors adopted to describe the molecular tensors $\boldsymbol{q}$ and $\boldsymbol{b}$ in Eq. (21).

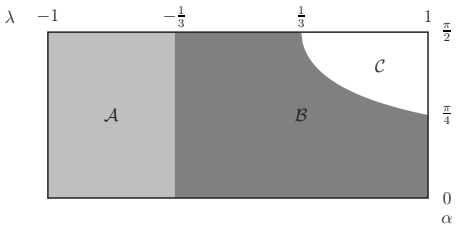

FIG. 3. The order parameter space $\mathcal{P}:\{(\lambda,\alpha):\lambda\in[-1,1],\ \alpha\in[0,\frac{\pi}{2}]\}$ is split for later reference in the subregions $\mathcal{A}$, $\mathcal{B}$, and $\mathcal{C}$. The boundary separating $\mathcal{B}$ from $\mathcal{C}$ in $\mathcal{P}$ is described by Eq. (B7).

$$H_{\rm dip}=U_0\left\{\frac{4}{3}\cos^2\alpha\boldsymbol{m}\cdot\boldsymbol{m}'+\left(\lambda+\frac{1}{3}\right)\sin\alpha\cos\alpha(\boldsymbol{e}\cdot\boldsymbol{m}'+\boldsymbol{e}'\cdot\boldsymbol{m})+2\left(\lambda-\frac{1}{3}\right)\sin^2\alpha\boldsymbol{e}\cdot\boldsymbol{e}'\right\}. \tag{23}$$

It readily follows from Eq. (23) that, for $\alpha=0$, $H_{\rm dip}$ is minimized by the antiparallel configuration $\boldsymbol{m}'=-\boldsymbol{m}$, no matter how $(\boldsymbol{e},\boldsymbol{e}_\perp)$ is oriented relative to $(\boldsymbol{e}',\boldsymbol{e}'_\perp)$, and so the interaction is *repulsive*. It is remarkable that the antinematic interaction described by $H_{\rm dip}$ for $\alpha=0$ is not affected by the biaxial shape of the molecules; this might be a consequence of our linear approximation for the molecular shape in Eq. (10): for $\alpha=0$, molecular biaxiality must be a second order effect in ε. For $\alpha=\frac{\pi}{2}$ and $\lambda<\frac{1}{3}$, the global minimizer of $H_{\rm dip}$ is the parallel configuration $\boldsymbol{e}'=\boldsymbol{e}$, and so the interaction is *attractive*. For $\alpha=\frac{\pi}{2}$ and $\lambda>\frac{1}{3}$, the minimizer of $H_{\rm dip}$ is the antiparallel configuration $\boldsymbol{e}'=-\boldsymbol{e}$. For $\alpha=\frac{\pi}{2}$ and $\lambda=\frac{1}{3}$, $H_{\rm dip}$ vanishes identically: steric hindrance compensates exactly electric dipolar interaction. Another limiting case where $H_{\rm dip}$ is somewhat degenerate arises for $\lambda=1$: then, by Eqs. (22) and (23) becomes

$$H_{\rm dip}=\frac{4}{3}U_0\boldsymbol{\ell}\cdot\boldsymbol{\ell}',$$

which, for any $\alpha\in[0,\frac{\pi}{2}]$, is minimized in the antiparallel configuration $\boldsymbol{\ell}'=-\boldsymbol{\ell}$.

The interactions embodied by Eq. (23) when either $\alpha=0$, $\alpha=\frac{\pi}{2}$, or $\lambda=1$, be they attractive or repulsive, are all of the simplest dipolar nature, with a single unit vector representing the molecular state. We are here interested in the most general interactions expressed by Eq. (23), and so we show in Appendix B that when neither $\alpha=0$, nor $\alpha=\frac{\pi}{2}$, nor $\lambda=1$, $H_{\rm dip}$ can in general be expressed as the superposition of an attractive and a repulsive component, which makes it *partly* repulsive, in the terminology adopted in [44]. In Appendix B, we also give all the mathematical details needed to identify the *repulsive dimension* associated with $H_{\rm dip}$.

To evaluate the *degree of polarization* Π of a pair of molecules in the ground state of $H_{\rm dip}$, we define

$$\Pi:=\frac{1}{2}|\boldsymbol{\ell}+\boldsymbol{\ell}'|. \tag{24}$$

It is easily shown by combining Eqs. (22) and (B10) that

$$\Pi=\sqrt{\frac{1-\cos 2(\chi+\alpha)}{2}}, \tag{25}$$

where $\pi-2(\chi+\alpha)$ is the angle that $\boldsymbol{\ell}'$ makes with $\boldsymbol{\ell}$ in the configuration that minimizes $H_{\rm dip}$. By use of Eq. (B8), we have drawn in Fig. 4 the graph of Π. This is discontinuous at the point $(\frac{1}{3},\frac{\pi}{2})$ on the boundary of the parameter space $\mathcal{P}$. The graph of Π also suggests that the ground state of the interaction $H_{\rm dip}$ would promote the highest degree of polarization for $\lambda\in[-1,\frac{1}{3}[$ and $\alpha=\frac{\pi}{2}$. The mean-field analysis presented in the following section will show to what extent

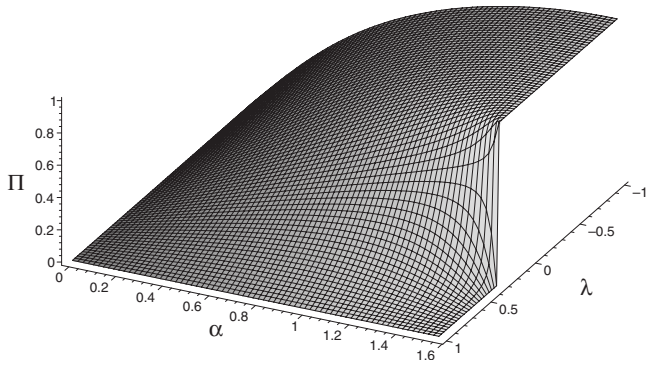

FIG. 4. The microscopic degree of polarization Π in the ground state of $H_{\rm dip}$, as given by Eq. (25), plotted over the parameter space $\mathcal{P}$. Π is a smooth function away from the point $(\frac{1}{3},\frac{\pi}{2}) \in \partial\mathcal{P}$.

the microscopic prediction for the highest polarization state based on Π is confirmed by an estimate based on the macroscopic free energy.

IV. MEAN-FIELD MODEL

In building our-mean field model for polar nematics based on the interaction Hamiltonian $H_{\rm dip}$, whose ground state has been shown to promote polarity in appropriate regions of the parameter space, we apply the general theory put forward in [44] for partly repulsive interactions.

A. Indefinite mean-field free energy

It is essential to our program to identify the macroscopic variables that describe the condensed phases along with their possible polarity. Following [54], we introduce the vector order parameters

$$\boldsymbol{M} := \langle \boldsymbol{m} \rangle \quad \text{and} \quad \boldsymbol{E} := \langle \boldsymbol{e} \rangle, \tag{26}$$

where $\langle \cdot \rangle$ denotes the appropriate ensemble average, which in our setting is to be computed relative to the one-particle distribution function ρ_0 of the mean-field approximation.

A condensed phase is *uniaxial* if either $\boldsymbol{M}=\boldsymbol{0}$ or $\boldsymbol{E}=\boldsymbol{0}$, or if $\boldsymbol{M} \| \boldsymbol{E}$, whereas it is *biaxial* if $\boldsymbol{M} \neq \boldsymbol{0}$ and $\boldsymbol{E} \neq \boldsymbol{0}$ and $\boldsymbol{M} \nparallel \boldsymbol{E}$. Both phases are indeed polar for $(\lambda, \alpha) \in \mathring{\mathcal{P}}$, as the ensemble dipole moment $\boldsymbol{P}$ normalized to the molecular dipole moment p reads as

$$\boldsymbol{P} := \langle \ell \rangle = \cos\, \alpha \boldsymbol{M} + \sin\, \alpha \boldsymbol{E}. \tag{27}$$

In principle, to represent both vectors $\boldsymbol{M}$ and $\boldsymbol{E}$ in an arbitrarily given frame $(\boldsymbol{e}_x, \boldsymbol{e}_y, \boldsymbol{e}_z)$, we should introduce three scalar order parameters for each vector. However, $\boldsymbol{M}$ and $\boldsymbol{E}$ define a plane. Whenever they are not parallel, we can assume this plane to be identified with $(\boldsymbol{e}_x, \boldsymbol{e}_z)$, and so we introduce the scalar order parameters (t,u,v,w) defined by

$$\boldsymbol{M} = t\boldsymbol{e}_x + u\boldsymbol{e}_z, \tag{28a}$$

$$\boldsymbol{E} = v\boldsymbol{e}_x + w\boldsymbol{e}_z. \tag{28b}$$

Correspondingly, by Eq. (27),

$$\boldsymbol{P} = P_x \boldsymbol{e}_x + P_z \boldsymbol{e}_z, \tag{29}$$

where

$$P_x = t\, \cos\, \alpha + v\, \sin\, \alpha, \tag{30a}$$

$$P_z = u\, \cos\, \alpha + w\, \sin\, \alpha. \tag{30b}$$

Since both $\boldsymbol{m}$ and $\boldsymbol{e}$ are unit vectors, it is an easy consequence of Eq. (26) that all scalar order parameters (t,u,v,w) are bound to range in the interval $[-1,1]$.

The assumption that neither $\boldsymbol{M}$ nor $\boldsymbol{E}$ can leave the plane $(\boldsymbol{e}_x, \boldsymbol{e}_z)$ in the different transitions possibly associated with phase transformations is to be confirmed *a posteriori* by computing the y-components M_y and E_y of $\boldsymbol{M}$ and $\boldsymbol{E}$ relative to the one-particle distribution function ρ_0 expressed in terms of (t,u,v,w): though finding M_y and E_y negligible will by no means be a proof of the validity of our assumption, it will provide evidence for the consistency of our model.

Following [44], we write the one-particle Hamiltonian H_0 (scaled to U_0) corresponding to the interaction Hamiltonian $H_{\rm dip}$ in Eq. (23) as

$$\begin{aligned} H_0(\boldsymbol{M},\boldsymbol{E};\boldsymbol{m},\boldsymbol{e}) = {} & \frac{4}{3}\cos^2\, \alpha \boldsymbol{M}\cdot\boldsymbol{m} \\ & + \left(\lambda + \frac{1}{3}\right) \sin\, \alpha\, \cos\, \alpha (\boldsymbol{M}\cdot\boldsymbol{e} + \boldsymbol{E}\cdot\boldsymbol{m}) \\ & + 2\left(\lambda - \frac{1}{3}\right) \sin^2\, \alpha \boldsymbol{E}\cdot\boldsymbol{e} \\ & - \frac{1}{2}\left[\frac{4}{3}\cos^2\, \alpha M^2\right. \\ & + 2\left(\lambda + \frac{1}{3}\right) \sin\, \alpha\, \cos\, \alpha \boldsymbol{M}\cdot\boldsymbol{E} \\ & \left. + 2\left(\lambda - \frac{1}{3}\right) \sin^2\, \alpha E^2\right]. \end{aligned} \tag{31}$$

The one-particle distribution function ρ_0 associated with H_0 is then

$$\rho_0(\boldsymbol{M},\boldsymbol{E};\beta,\omega) := \frac{1}{Z_0} e^{-\beta H_0[\boldsymbol{M},\boldsymbol{E},\boldsymbol{m}(\omega),\boldsymbol{e}(\omega)]}, \tag{32}$$

where $\omega=(\vartheta,\varphi,\psi)$ is the triple of angles adopted to describe the molecular orientation in the frame $(\boldsymbol{e}_x, \boldsymbol{e}_y, \boldsymbol{e}_z)$,

$$\beta := \frac{U_0}{k_B T}, \tag{33}$$

with k_B the Boltzmann constant, is the dimensionless inverse temperature and

$$Z_0(\boldsymbol{M},\boldsymbol{E};\beta) := \frac{1}{8\pi^2} \int_{\mathbb{T}} e^{-\beta H_0[\boldsymbol{M},\boldsymbol{E};\boldsymbol{m}(\omega),\boldsymbol{e}(\omega)]} d\omega \tag{34}$$

is the *partition function*. In Eq. (34), $\mathbb{T}$ is the *orientation torus*, a three-dimensional manifold with measure $d\omega = \sin\, \vartheta d\vartheta d\varphi d\psi$. Specifically, we represent $\boldsymbol{m}$ and $\boldsymbol{e}$ as in [50],

$$\boldsymbol{m}(\omega) = \cos\varphi \sin\vartheta \boldsymbol{e}_x + \sin\varphi \sin\vartheta \boldsymbol{e}_y + \cos\vartheta \boldsymbol{e}_z, \tag{35a}$$

$$\boldsymbol{e}(\omega) = (\cos\psi\cos\varphi\cos\vartheta - \sin\psi\sin\varphi)\boldsymbol{e}_x + (\cos\psi\sin\varphi\cos\vartheta + \sin\psi\cos\varphi)\boldsymbol{e}_y - \cos\psi\sin\vartheta\boldsymbol{e}_z. \tag{35b}$$

The one-particle (dimensionless) free energy F_0 is defined in terms of Z_0 as

$$F_0(\boldsymbol{M},\boldsymbol{E};\beta) := -\frac{1}{\beta}\ln Z_0(\boldsymbol{M},\boldsymbol{E};\beta). \tag{36}$$

As proved in [44], for every given $\beta>0$, the equilibrium points of F_0 represent the solutions to the self-compatibility equations generated by Eq. (26) upon computing the ensemble averages appearing there with respect to ρ_0 in Eq. (32). The theory developed in [44] shows that, for partly repulsive Hamiltonians such as H_{dip}, the equilibrium points of F_0 are all saddle points and F_0 is neither bounded from below nor from above: for given β, the mean-field approximation to the minimum of the two-particle free energy F associated to H_{dip} is the least critical value of F_0, which is not a minimum of F_0. To identify the least critical value of F_0 through a bifurcation analysis moving for increasing β from the isotropic phase, where both $\boldsymbol{M}$ and $\boldsymbol{E}$ vanish, a local stability criterion is required that singles out the critical values of F_0 that can legitimately compete to deliver its least critical value. As shown in [44], such a criterion requires the Hessian matrix $\mathbb{H}$ at a critical point of F_0 to possess a number of negative eigenvalues equal to the repulsive dimension n^-, which is defined as the number of independent scalar order parameters needed to represent the mean-field average of the repulsive microscopic variable. Having identified this latter in Appendix B as the molecular unit vector $\boldsymbol{m}^*$, it follows from Eqs. (B1b), (26), and (28) that $n^-=2$ in the present representation of $\boldsymbol{M}$ and $\boldsymbol{E}$.

We are now in a position to express F_0 in Eq. (36) as a function f of the scalar order parameters (t,u,v,w),

$$f(t,u,v,w;\beta) = -\left[\frac{2}{3}\cos^2\alpha(t^2+u^2) + \left(\lambda+\frac{1}{3}\right)\sin\alpha\cos\alpha(tv+uw) + \left(\lambda-\frac{1}{3}\right)\sin^3\alpha(v^2+w^2)\right] - \frac{1}{\beta}\ln\frac{1}{8\pi^2}\int_{\mathrm{T}} e^{\beta g(t,u,v,w;\omega)}d\omega, \tag{37}$$

where

$$g(t,u,v,w;\omega) := \frac{4}{3}\cos^2\alpha(t\cos\varphi\sin\vartheta + u\cos\vartheta) + \left(\lambda+\frac{1}{3}\right)\sin\alpha\cos\alpha[t(-\sin\psi\cos\varphi + \cos\psi\cos\varphi\cos\vartheta) - u\cos\psi\sin\vartheta + v\cos\varphi\sin\vartheta + w\cos\vartheta] + 2\left(\lambda-\frac{1}{3}\right)\sin^2\alpha[v(\cos\psi\cos\varphi\cos\vartheta - \sin\psi\sin\varphi) - w\cos\psi\sin\vartheta]. \tag{38}$$

The equilibrium equations that identify the critical points of f can be cast in the form

$$\frac{4}{3}\cos^2\alpha t + \left(\lambda+\frac{1}{3}\right)\sin\alpha\cos\alpha v - \frac{Z_t}{Z} = 0, \tag{39a}$$

$$\frac{4}{3}\cos^2\alpha u + \left(\lambda+\frac{1}{3}\right)\sin\alpha\cos\alpha w - \frac{Z_u}{Z} = 0, \tag{39b}$$

$$2\left(\lambda-\frac{1}{3}\right)\sin^2\alpha v + \left(\lambda+\frac{1}{3}\right)\sin\alpha\cos\alpha t - \frac{Z_v}{Z} = 0, \tag{39c}$$

$$2\left(\lambda-\frac{1}{3}\right)\sin^2\alpha w + \left(\lambda+\frac{1}{3}\right)\sin\alpha\cos\alpha u - \frac{Z_w}{Z} = 0, \tag{39d}$$

where

$$Z(t,u,v,w;\beta) := \int_{\mathrm{T}} e^{-\beta g(t,u,v,w;\omega)}d\omega \tag{40}$$

is the *reduced* partition function and

$$Z_x(t,u,v,w;\beta) := \int_{\mathrm{T}} \frac{\partial g}{\partial x} e^{-\beta g(t,u,v,w;\omega)}d\omega, \tag{41}$$

for any scalar order parameter x.

The equilibrium equations (39) suffer from a severe degeneracy. Rotating both $\boldsymbol{M}$ and $\boldsymbol{E}$ by the same angle about $\boldsymbol{e}_y$ does indeed leave F_0 unchanged, since this is a frame-indifferent function. Correspondingly, each critical point of f in the variables (t,u,v,w) is transformed into another where f attains the same value by the transformation that acts on the pairs (t,u) and (v,w) as one and the same rotation in the plane; this associates a full orbit to every critical point of f. To remove such a degeneracy from the equilibrium manifold of f, we constrain our search for its critical points to $t=0$, thus selecting a single point in the equilibrium orbit, effectively defining $\boldsymbol{e}_z$ as the direction of $\boldsymbol{M}$. Since requiring that an equilibrium point of f occurs at $t=0$ is equivalent to enforcing the self-consistency condition

$$\int_{\mathrm{T}} \cos\varphi\sin\vartheta e^{-\beta g_0(u,v,w;\omega)}d\omega = 0, \tag{42}$$

where

$$g_0(u,v,w;\omega) := g(0,u,v,w;\omega), \tag{43}$$

we now explore the consequences of setting $t=0$ into Eq. (39), while requiring Eq. (42) to be satisfied. It is easily seen that Eqs. (39a) and (39c) then become equivalent and Eqs. (39b)–(39d) can also be interpreted as equilibrium equations for the function

$$f_0(u,v,w;\beta) := f(0,u,v,w;\beta) \tag{44}$$

on which the constraint Eq. (42) is imposed as a further requirement. This also amounts to find the free equilibrium points in (u,v,w) of the *extended* function

$$f_0^*(u,v,w;\beta) := f_0(u,v,w;\beta) + \mu \int_{\mathrm{T}} \cos\varphi \sin\vartheta e^{-\beta g_0(u,v,w;\omega)} d\omega, \tag{45}$$

where μ plays the role of a Lagrange multiplier to be determined with the aid of Eq. (42), but with the proviso that only such equilibrium points (u,v,w) for which $\mu=0$ correspond to solutions $(0,u,v,w)$ of Eq. (39). Equivalently, the equilibrium point (u,v,w) solves the overdetermined system comprising the equilibrium equations for f_0 and Eq. (42).

Eventually, the validity of our approach is subject to the compatibility between the representation in Eq. (27) for the macroscopic averages $\boldsymbol{M}$ and $\boldsymbol{E}$ and the corresponding one-particle distribution function ρ_0 in Eq. (32). In particular, such a compatibility requires that

$$0 = M_y = \frac{1}{z_0}\int_{\mathrm{T}} \sin\varphi \sin\vartheta e^{-\beta g_0} d\omega, \tag{46a}$$

$$0 = E_y = \frac{1}{z_0}\int_{\mathrm{T}} (\cos\psi \sin\varphi \cos\vartheta + \sin\psi \cos\varphi) e^{-\beta g_0} d\omega, \tag{46b}$$

where

$$z_0(u,v,w;\beta) := Z(0,u,v,w;\beta). \tag{47}$$

The details of our strategy to solve Eqs. (39), freed from their degeneracy, are given in Appendix C, where the stability of the equilibrium solutions is also characterized.

B. Bifurcation diagrams

We performed a numerical bifurcation analysis starting from the trivial solution $u=v=w=0$, which corresponds to the isotropic phase. Upon increasing β, we found a new stable solution branch emanating off the trivial solution at $\beta=\beta_c$ [see Eq. (C2) in Appendix C], where the trivial solution becomes unstable. We found that along the bifurcated branch not only t but also v vanishes to within our numerical precision, while the functions $u(\beta)$ and $w(\beta)$ are in a ratio ρ that appears to be independent of β, to within the same numerical precision, while it takes different values for different model parameters $(\lambda,\alpha) \in \mathcal{P}$. Figure 5 shows typical bifurcation diagrams, obtained for (λ,α) in the three regions $\mathcal{A}$, $\mathcal{B}$, and $\mathcal{C}$ of Fig. 3; they all show the classical pitchfork bifurcation with exchange of stability at $\beta=\beta_c$.

In all the computations we performed, for (λ,α) in either $\mathcal{A}$, $\mathcal{B}$, or $\mathcal{C}$, we systematically found M_y, E_y, and μ negli-

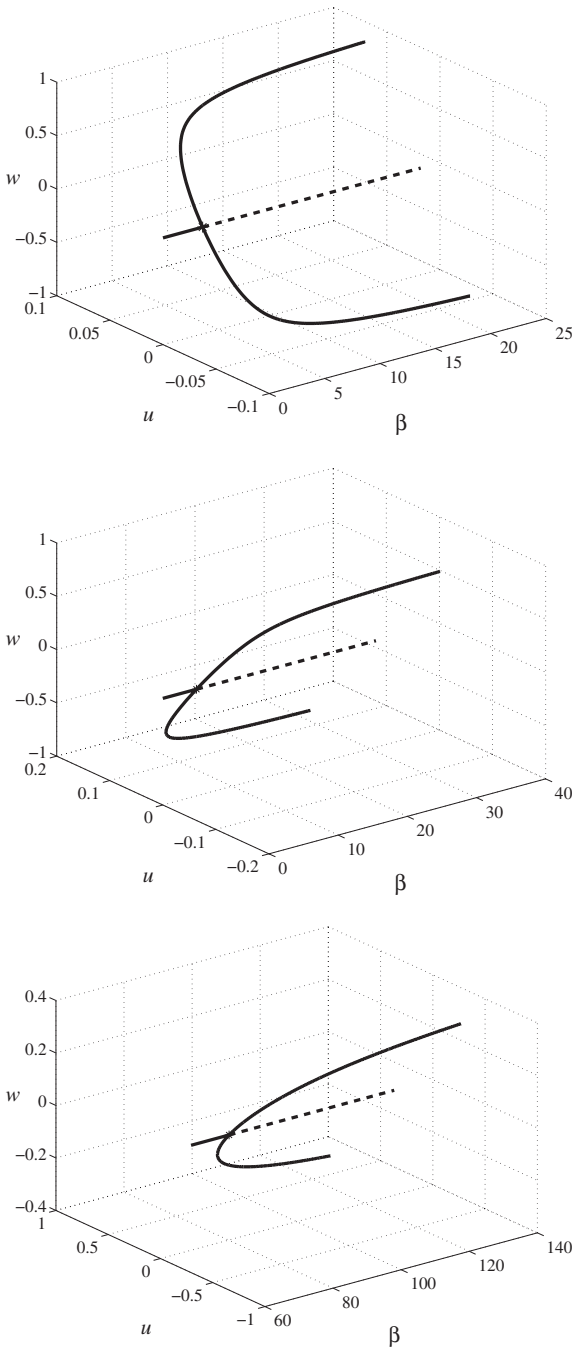

FIG. 5. Bifurcation diagrams for the scalar order parameters u and w against the reciprocal dimensionless temperature β. Stable branches are represented by solid lines, while unstable branches are represented by dashed lines. At the critical value $\beta=\beta_c$, which agrees with the value delivered by Eq. (C2), a second order transition takes place: the isotropic phase becomes unstable, and stability occurs at a polar uniaxial stable phase with $t=v=0$ and $u/w=\rho$, in complete agreement with Eq. (49). (a) Typical bifurcation diagram in region $\mathcal{A}$, parameters used are $\lambda=-\frac{1}{2}$ and $\alpha=\frac{\pi}{4}$. Here $\beta_c=3.5802$, $\rho=0.0554$; the dominant order parameter is w. (b) Typical bifurcation diagram in region $\mathcal{B}$, parameters used are $\lambda=0$ and $\alpha=\frac{2}{5}\pi$. Here $\beta_c=4.8708$, $\rho=-0.1318$; the dominant order parameter is w. (c) Typical bifurcation diagram in region $\mathcal{C}$, parameters used are $\lambda=\frac{4}{9}$ and $\alpha=\frac{7}{16}\pi$. Here $\beta_c=80.1608$, $\rho=-1.6879$; the dominant order parameter is u.

gible, to within our numerical precision. By Eq. (27), we then conclude that the condensed phase represented by these scalar order parameters is *uniaxial*, as both $\boldsymbol{M}$ and $\boldsymbol{E}$ are along $\boldsymbol{e}_z$. By Eqs. (29), the polarization $\boldsymbol{P}$ is also along $\boldsymbol{e}_z$. Since, as far as we could explore, this conclusion applies everywhere in the interior $\mathring{\mathcal{P}}$ of the parameter space, we are thus led to conjecture that the condensed phases predicted by our model are uniaxial for all $(\lambda,\alpha)\in\mathring{\mathcal{P}}$, so that a single scalar order parameter, either u or w, would indeed suffice to describe them. Below, we assume this conjecture as valid and we explore its consequences.

C. Maximum polarization

Here we show that the only ordered equilibrium phase predicted by our model is polar uniaxial, and we learn how to choose the parameters (λ,α) to maximize the phase polarization. The numerical evidence we collected makes us believe that the only equilibrium solutions for f are such that

$$t=\rho v \quad \text{and} \quad u=\rho w, \tag{48}$$

with ρ depending only on (λ,α).

The situation we envisage is similar to that encountered in the classical Maier-Saupe theory. Allowing the mean-field ensemble average $\mathbf{Q}$ of the microscopic uniaxial tensor $\mathbf{q}$ to be potentially biaxial does not lead to any more solutions to the equilibrium equations for the resulting mean-field free energy F_0 than were already found in the seminal paper of Maier and Saupe [26] under the assumption that $\mathbf{Q}$ be uniaxial. As predictable as this result may seem, it has only recently been proved analytically [55–57].

Having chosen $t\equiv 0$ to lift the degeneracy of f under rotations, we also obtain from Eq. (48) that $v\equiv 0$. At the bifurcation point, where $\beta=\beta_c$, u and w satisfy the linear system

$$H_{uu}u+H_{uw}w=0,$$

$$H_{uw}u+H_{ww}w=0,$$

where H_{uu}, H_{uw}, and H_{ww} are components of the Hessian matrix of f, see Eq. (C1) in Appendix C. Under the assumption in Eq. (48), we then obtain an analytic expression for ρ,

$$\rho(\lambda,\alpha)=-\frac{H_{uw}}{H_{ww}}=-\frac{(3\lambda+1)\sin\alpha\{9+\beta_c[4\cos^2\alpha+2(3\lambda-1)\sin^2\alpha]\}}{4\cos\alpha\left\{9+\beta_c\left[4\cos^2\alpha+\frac{1}{4}(3\lambda+1)^2\sin^2\alpha\right]\right\}}, \tag{49}$$

where β_c is given by Eq. (C2) as a function of (λ,α).

The analysis of the function ρ in Eq. (49) shows that it vanishes for $\lambda=-\frac{1}{3}$ and on two segments on $\partial\mathcal{P}$, namely, $\{(\lambda,\alpha):\lambda\in[-1,1],\alpha=0\}$ and $\{(\lambda,\alpha):\lambda\in[-1,\frac{1}{3}[,\alpha=\frac{\pi}{2}\}$; the whole nodal set of ρ is marked in Fig. 10 by bold dots. In particular, ρ is positive in $\mathcal{A}$, where it stays below 1, and negative in the interior of $\mathcal{P}\backslash\mathcal{A}$, where it equals -1 precisely along the line $\alpha=\alpha_c$ that marks the boundary between $\mathcal{B}$ and $\mathcal{C}$: more specifically, $-1<\rho<0$ in $\mathcal{B}$ and $\rho<-1$ in $\mathcal{C}$. Moreover, ρ diverges to $-\infty$ upon approaching the segment $\{(\lambda,\alpha):\lambda\in]\frac{1}{3},1],\alpha=\frac{\pi}{2}\}$ on $\partial\mathcal{P}$ and it approaches the function $-\tan\alpha$ as λ approaches 1. Since both u and w range in the interval $[-1,1]$, this shows that u is the dominant order parameter in $\mathcal{C}$, while w is the dominant order parameter in $\mathcal{P}\backslash\mathcal{C}$. Furthermore, u and w have the same sign in $\mathcal{A}$ and opposite signs in the interior of $\mathcal{P}\backslash\mathcal{A}$. Clearly, reversing the sign of both u and w does not change the phase, as both vectors $\boldsymbol{M}$ and $\boldsymbol{E}$ simply get reversed, but reversing the sign of their ratio ρ affects the phase polarity $\boldsymbol{P}$.

Assuming that the dominant order parameter saturates to 1 as β grows away from β_c, which was indeed the case for all our numerical solutions, we can derive from Eq. (27) with Eq. (48) an explicit expression for the measure of *saturated* polarization,

$$\mathsf{P}(\lambda,\alpha):=\lim_{\beta\to\infty}|P_z|=\begin{cases}\sin\alpha+\rho\cos\alpha & \text{in } \mathcal{P}\backslash\mathcal{C},\\ \left|\cos\alpha+\dfrac{1}{\rho}\sin\alpha\right| & \text{in } \mathcal{C},\end{cases} \tag{50}$$

where ρ is as in Eq. (49). The graph of the function P in Eq. (50) is depicted in Fig. 6; it shows that the largest saturated polarization is attained for $\lambda\in[-1,\frac{1}{3}[$ and $\alpha=\frac{\pi}{2}$. The graph of P is similar in its appearance to the graph of the microscopic degree of polarization Π derived through Eq. (25) from the ground state of H_{dip} and shown in Fig. 4 above. To illustrate quantitatively both similarities and differences between P and Π we draw in Fig. 7 the graph of $\Delta:=\Pi-\mathsf{P}$. It clearly indicates that P and Π differ mainly around the boundary separating $\mathcal{B}$ from $\mathcal{C}$.

The above analysis indicates that for the interaction Hamiltonian H_{dip} studied in this paper the polar nematic transition takes place at the least possible temperature and establishes the largest polarization at saturation, if $\lambda=-1$ and $\alpha=\frac{\pi}{2}$. In the light of Sec. III A above, this means that among all molecules whose shape is described by Eqs. (14) and (20) the most efficient ones in promoting a polar nematic phase are disklike, symmetric about the axis of their permanent dipole moment.

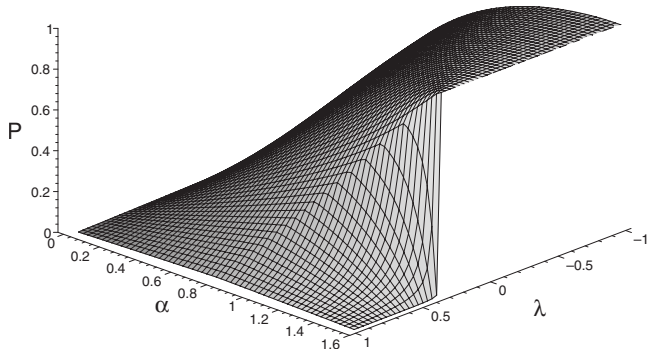

FIG. 6. The graph of the saturated polarization P defined by Eq. (50), plotted over the parameter space $\mathcal{P}$. P is a continuous function in $\mathring{\mathcal{P}}$, exhibiting a discontinuity at $(\frac{1}{3},\frac{\pi}{2}) \in \partial\mathcal{P}$. It fails to be differentiable along the line $\alpha=\alpha_c(\lambda)$, see Eq. (B7), which separates $\mathcal{B}$ from $\mathcal{C}$ in Fig. 3.

V. CONCLUSION

We employed a mean-field theory to explore the possible occurrence of a polar nematic phase comprising polar molecules biaxial in shape. Our program also conceived the possibility that the resulting phase were biaxial, as an effect of the mutual steric hindrance between the constituting molecules.

This is perhaps the point where our approach differs the most from other theoretical attempts to describe the molecular mechanism behind the possible occurrence of polar nematic phases: that we combine in one and the same theory the attractive, long-range dipolar forces that promote the molecular alignment and the repulsive, short-range steric forces that interfere with the former to the point of counterbalancing their aligning effect. Our analysis was based on the steric tensor $\mathbf{S}_{\mathcal{R}^*}$, a second-rank tensor depending on the molecular excluded region $\mathcal{R}^*$, which within our theory embodies the steric component of the molecular interaction.

We were able to compute $\mathbf{S}_{\mathcal{R}^*}$ analytically only in the limit where the molecular shape $\mathcal{R}$ is a spheroid, obtained as a small biaxial deformation of a sphere. Within this limit, we determined explicitly the pair-potential H_{dip} representing the dipolar interaction along with the steric effects that modify it; the analysis of its ground state revealed that it is partly repulsive. Applying to H_{dip} the general mean-field theory for partly repulsive Hamiltonians, we obtained the equilibrium phases for all temperatures T and for all choices of the model parameters (λ,α).

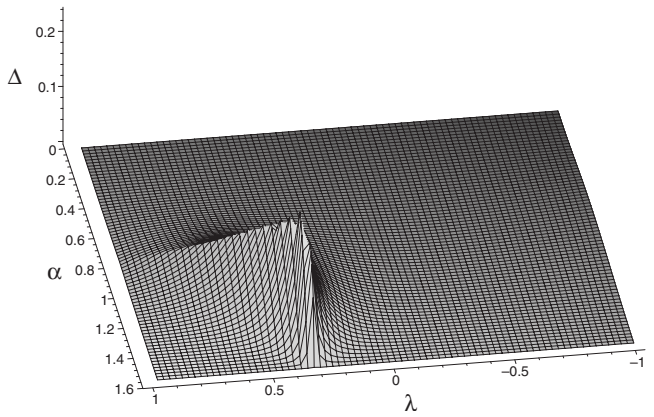

FIG. 7. The graph of the difference $\Delta := \Pi - \mathsf{P}$ between the microscopic degree of polarization Π in the ground state of H_{dip} and the macroscopic saturated polarization defined by Eq. (50). Δ is appreciably different from zero only along the boundary separating the regions $\mathcal{B}$ and $\mathcal{C}$ in $\mathcal{P}$, see Fig. 3.

We found that there is a critical temperature T_c such that the equilibrium phase is isotropic for $T>T_c$ and nematic, at the same time polar and uniaxial, for $T<T_c$. The equilibrium solutions computed in our work suggested that the condensed nematic polar phase can indeed be described by a single scalar order parameter. The phase transition taking place at $T=T_c$ is second order and the corresponding bifurcation diagram has a typical pitchfork appearance with the usual associated exchange of stability. The analysis of the dependence of T_c on the model parameters revealed that T_c is maximal when the constituting molecules are disklike in shape with their permanent dipole moment $\boldsymbol{p}$ along the symmetry axis. Thus, for such molecules, the nematic transition should be less likely to be preempted by other transitions also involving some degree of spatial ordering, such as the smectic transition, which were not considered in our study. The same disklike molecules would promote the largest polarization of the condensed phase at saturation. Quantitatively, placing $\boldsymbol{p}$ along the axis of a prolate molecule would result in a transition temperature T_c four times smaller than the one expected when $\boldsymbol{p}$ is placed along the axis of an oblate molecule [see Eq. (C3) in Appendix C]. This conclusion, which we made precise within a specific class of molecular shapes, had already been anticipated in [34] through an intuitive reasoning. It suggests a general criterion to engineer polar molecules more likely to give rise to a polar nematic phase.

Our model failed to produce a polar biaxial phase. A possible reason for this could be the restriction of the molecular shape to spheroids. A further study where molecules are not spheroidal is presently under way; it relies on a general computational method to construct the steric tensor for dipolar molecules with a generic convex shape [58]. The ultimate objective of this study is to identify the molecular shape that in a given, not too narrow family of model shapes would promote the transition to a polar nematic phase, possibly biaxial, at the largest temperature and with the largest saturation polarization.

ACKNOWLEDGMENTS

F.B. acknowledges the Italian GNFM-INdAM for financial support of his work through the grant "Progetto Giovani 2008: *Modelli multiscala per fluidi nanostrutturati*." We wish to thank an anonymous reviewer of this paper, whose knowledgeable criticism has prompted a better understanding of our work.

APPENDIX A: STAGGERED CONFIGURATIONS

We show here that the small deformation of the spherical shape represented by Eq. (10) is sufficient to make both the

parallel and the antiparallel dipolar configurations staggered, that is, such that the minimum of U_{dip} is attained when the intermolecular vector is neither parallel nor orthogonal to the dipoles.

By replacing r in Eq. (1) with the distance of closest approach u^* in Eq. (12), also with the aid of Eq. (14), we write U_{dip} as $U_{\parallel}$ or $U_{\perp}$, according as to whether $\ell' = \ell$ or $\ell' = -\ell$. Representing $\boldsymbol{e}_r$ in the form

$$\boldsymbol{e}_r = \cos\vartheta \boldsymbol{m} + \sin\vartheta\cos\varphi \boldsymbol{e} + \sin\vartheta\sin\varphi \boldsymbol{e}_{\perp}$$

and making use of Eqs. (20), (21a), (21b), and (22), we express $U_{\parallel}$ and $U_{\perp}$ as functions of ϑ and φ:

$$U_{\parallel} = \frac{p^2}{32\pi\epsilon_0 R^3} U \quad \text{and} \quad U_{\perp} = -U_{\parallel},$$

with

$$U(\vartheta,\varphi) := \frac{1 - 3(\cos\alpha\cos\vartheta + \sin\alpha\sin\vartheta\cos\varphi)^2}{\left\{1 + \varepsilon\left[\frac{2}{3}\cos^2\vartheta + \left(\lambda - \frac{1}{3}\right)\sin^2\vartheta\cos^2\varphi - \left(\lambda + \frac{1}{3}\right)\sin^2\vartheta\sin^2\varphi\right]\right\}^3}. \tag{A1}$$

It is easily checked that the function U is invariant under the transformation $(\vartheta,\varphi)\mapsto(\pi-\vartheta,\varphi+\pi)$, which simply amounts to exchange the particles in the interacting pair.

For $\varepsilon=0$, U possesses both $(\alpha,0)$ and $(\alpha+\frac{\pi}{2},0)$ as critical points, being the former its absolute minimizer. They correspond to the parallel and antiparallel dipolar configurations, with $\ell \| \boldsymbol{e}_r$ in the former and $\ell \perp \boldsymbol{e}_r$ in the latter. Expanding U up to second order in ε, one finds that for every $\alpha \in]0,\frac{\pi}{2}[$, the critical points $(\alpha,0)$ and $(\alpha+\frac{\pi}{2},0)$ migrate into $(\vartheta_\varepsilon,\varphi_\varepsilon)$, with

$$\vartheta_\varepsilon = \alpha + \varepsilon(1-\lambda)\sin 2\alpha + o(\varepsilon), \quad \varphi_\varepsilon = o(\varepsilon)$$

and

$$\vartheta_\varepsilon = \alpha + \frac{\pi}{2} - \frac{\varepsilon}{2}(1-\lambda)\sin 2\alpha + o(\varepsilon), \quad \varphi_\varepsilon = o(\varepsilon),$$

respectively, which shows how both parallel and antiparallel configurations are now staggered at first order in ε. Clearly, as already remarked in the text, the absolute minimizer of U_{dip} is the staggered parallel configuration.

APPENDIX B: REPULSIVE DIMENSION

To illustrate better the partly repulsive nature of the interaction described by Eq. (23) and to identify the dimension of its repulsive component, we write H_{dip} in Eq. (23) as the sum of two simple dipolar interactions. To this end, we introduce in each molecule a different set of reference unit vectors, $(\boldsymbol{e}^*,\boldsymbol{m}^*)$, rotated by the angle χ^* with respect to $(\boldsymbol{e},\boldsymbol{m})$,

$$\boldsymbol{e}^* := \cos\chi^* \boldsymbol{e} + \sin\chi^* \boldsymbol{m}, \tag{B1a}$$

$$\boldsymbol{m}^* := -\sin\chi^* \boldsymbol{e} + \cos\chi^* \boldsymbol{m}. \tag{B1b}$$

Correspondingly, for any other molecule in an interacting pair, the same unit vectors read as

$$\boldsymbol{e}^{*\prime} := \cos\chi^* \boldsymbol{e}' + \sin\chi^* \boldsymbol{m}', \tag{B2a}$$

$$\boldsymbol{m}^{*\prime} := -\sin\chi^* \boldsymbol{e}' + \cos\chi^* \boldsymbol{m}'. \tag{B2b}$$

It is easily seen that by use of (B1) and (B2) H_{dip} in (23) can be given the following equivalent form:

$$H_{\mathrm{dip}} = U_0\{a_m \boldsymbol{m}^* \cdot \boldsymbol{m}^{*\prime} + a_e \boldsymbol{e}^* \cdot \boldsymbol{e}^{*\prime}\}, \tag{B3}$$

provided that χ^* is defined by

$$\chi^* := -\frac{1}{2}\arctan\left[\frac{(1+3\lambda)\tan\alpha}{2 + (1-3\lambda)\tan^2\alpha}\right] \tag{B4}$$

and a_m and a_e are identified with

$$a_m = \frac{1}{3}(1+\cos 2\alpha)(1+\cos 2\chi^*) - \frac{1}{2}\left(\lambda + \frac{1}{3}\right)\sin 2\alpha \sin 2\chi^* + \frac{1}{2}\left(\lambda - \frac{1}{3}\right)(1-\cos 2\alpha)(1-\cos 2\chi^*) \tag{B5a}$$

and

$$a_e = \frac{1}{3}(1+\cos 2\alpha)(1-\cos 2\chi^*) + \frac{1}{2}\left(\lambda + \frac{1}{3}\right)\sin 2\alpha \sin 2\chi^* + \frac{1}{2}\left(\lambda - \frac{1}{3}\right)(1-\cos 2\alpha)(1+\cos 2\chi^*). \tag{B5b}$$

An easy but tedious computation shows that, with χ^* as in Eq. (B4),

$$a_m a_e = -(\lambda-1)^2 \sin^2\alpha \cos^2\alpha, \tag{B6}$$

and so, for either $\lambda \in [-1,1[$ and $\alpha \in]0,\frac{\pi}{2}[$, H_{dip} is partly repulsive, as either a_m or a_e is negative.

As is clear from Eq. (B1), the transformation $\chi^* \mapsto \chi^* + \frac{\pi}{2}$ maps $\boldsymbol{e}^*$ into $\boldsymbol{m}^*$ and $\boldsymbol{m}^*$ into $-\boldsymbol{e}^*$, while by Eq. (B5) a_m and a_e get correspondingly exchanged, so that H_{dip} in Eq. (B3) remains eventually unchanged. This shows that χ^* may suffer a jump by $\frac{\pi}{2}$, which necessarily produces both a discontinuity and a change in sign in both a_e and a_m, without affecting H_{dip}. With χ^* defined as in Eq. (B4), this actually occurs for

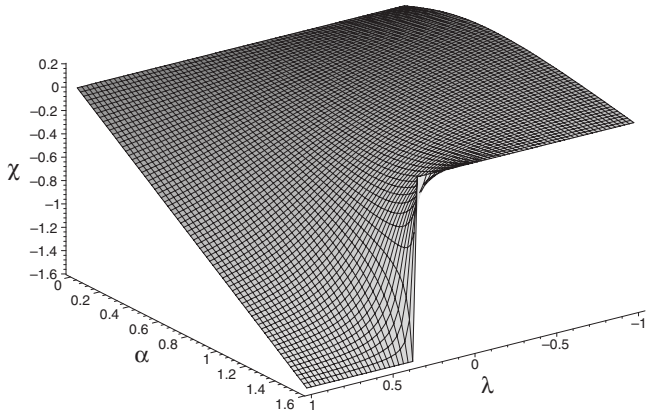

FIG. 8. The graph of the function χ defined in Eq. (B8) over the parameter space $\mathcal{P}$; χ is a smooth function away from the discontinuity for $\lambda=\frac{1}{3}$ and $\alpha=\frac{\pi}{2}$.

$$\alpha = \alpha_c(\lambda) := \arctan\sqrt{\frac{2}{3\lambda - 1}} \quad \text{and} \quad \frac{1}{3} < \lambda \leq 1, \tag{B7}$$

which marks the boundary of the open region $\mathcal{C}$ within the parameter space $\mathcal{P}:=\{(\lambda,\alpha):\lambda\in[-1,1],\alpha\in[0,\frac{\pi}{2}]\}$ depicted in Fig. 3. Whereas χ^* in Eq. (B4) converges to the limiting value $-\frac{\pi}{4}$ upon approaching the line $\alpha=\alpha_c(\lambda)$ in the interior of $\mathcal{P}\backslash\mathcal{C}$, it converges to $+\frac{\pi}{4}$ upon approaching the same line in the interior of $\mathcal{C}$; for χ^* as in Eq. (B4), $a_e>0$ and $a_m<0$ in $\mathcal{C}$, whereas $a_e<0$ and $a_m>0$ in the interior of $\mathcal{P}\backslash\mathcal{C}$. To avoid this annoying but immaterial discontinuity, which has no physical meaning, we redefine the function χ^* so as to make it continuous across the boundary between $\mathcal{C}$ and the interior of $\mathcal{P}\backslash\mathcal{C}$: we replace χ^* by χ defined as

$$\chi(\lambda,\alpha) := \begin{cases} \chi^*(\lambda,\alpha) & \text{for } (\lambda,\alpha)\in\mathcal{P}\backslash\mathcal{C}, \\ \chi^*(\lambda,\alpha)-\dfrac{\pi}{2} & \text{for } (\lambda,\alpha)\in\mathcal{C}. \end{cases} \tag{B8}$$

The graph of χ is presented in Fig. 8, which shows how χ is indeed a smooth function in the whole of the interior $\mathring{\mathcal{P}}$ of $\mathcal{P}$ and suffers a $\frac{\pi}{2}$-discontinuity at $\lambda=\frac{1}{3}$ and $\alpha=\frac{\pi}{2}$. The interior of $\mathcal{P}\backslash\mathcal{C}$ is further split into the open regions $\mathcal{A}$ and $\mathcal{B}$, separated by the line $\lambda=-\frac{1}{3}$ (see Fig. 3): χ is positive only in $\mathcal{A}$. We conclude that, with χ^* replaced by χ, $\boldsymbol{m}^*$ is the repulsive microscopic variable throughout $\mathring{\mathcal{P}}$, whereas $\boldsymbol{e}^*$ is the attractive one: the former minimizes the pair potential H_{dip} in the antiparallel configuration $\boldsymbol{m}^{*\prime}=-\boldsymbol{m}^*$, whereas the latter minimizes H_{dip} in the parallel configuration $\boldsymbol{e}^{*\prime}=\boldsymbol{e}^*$. According to [44], the *repulsive dimension* is defined by the number of independent scalar order parameters needed to represent the macroscopic ensemble average $\langle\boldsymbol{m}^*\rangle$. Since this is a vector in three-dimensional space, one would normally expect that such a dimension is 3; as shown in Sec. IV, it can be effectively reduced.

To bring the triple $(\boldsymbol{e},\boldsymbol{e}_\perp,\boldsymbol{m})$ identifying one molecule into the triple $(\boldsymbol{e}',\boldsymbol{e}'_\perp,\boldsymbol{m}')$ identifying the other molecule in the interacting pair so that H_{dip} attains its ground state everywhere in $\mathring{\mathcal{P}}$, we perform the rotation described by the equations

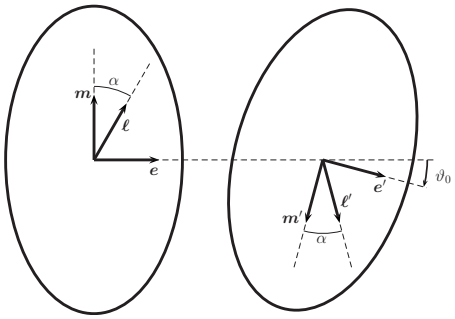

FIG. 9. Cartoon of two molecules in the ground state of H_{dip} in Eq. (23), for a choice of parameters (λ,α) in $\mathcal{P}\backslash\mathcal{A}$, see Fig. 3.

$$\boldsymbol{e}' = \cos\vartheta_0\boldsymbol{e} - \sin\vartheta_0\boldsymbol{m}, \tag{B9a}$$

$$\boldsymbol{e}'_\perp = -\boldsymbol{e}_\perp, \tag{B9b}$$

$$\boldsymbol{m}' = -\sin\vartheta_0\boldsymbol{e} - \cos\vartheta_0\boldsymbol{m} \tag{B9c}$$

and illustrated in Fig. 9, where the angle ϑ_0 is to be determined so that $\boldsymbol{m}^{*\prime}=-\boldsymbol{m}^*$ and $\boldsymbol{e}^{*\prime}=\boldsymbol{e}^*$. By rewriting these latter equations with the aid of Eq. (B9), we readily arrive at

$$\vartheta_0 = -2\chi. \tag{B10}$$

By the way χ is defined in Eq. (B8), which removes the meaningless discontinuity of χ^* across the boundary separating $\mathcal{B}$ from $\mathcal{C}$ in $\mathcal{P}$, ϑ_0 turns out to be positive in $\mathcal{P}\backslash\mathcal{A}$, as in the sketch shown in Fig. 9, and negative in $\mathcal{A}$.

APPENDIX C: BIFURCATION ANALYSIS

The trivial triple $(u,v,w,)=(0,0,0)$ corresponds to the isotropic phase. It is clearly nonpolar and it is a solution to the equilibrium problem for any $\beta>0$. The search for nontrivial equilibrium solutions $(0,u,v,w)$ of Eq. (39) was performed through a numerical bifurcation analysis of the equilibrium equations for f_0^*, with the aid of MATCONT,[2] a free software package which integrates into MATLAB.[3] This method was already employed in the bifurcation analysis of the equilibrium phases for nonpolar biaxial nematic liquid crystals [42,43,52,53]. Here our analysis was further complicated by the need of monitoring the Lagrange multiplier μ and the equilibrium values of M_y and E_y in Eq. (46) along all possible bifurcation branches, to ensure that they can be regarded as negligibly small.

In the light of our analysis of the partly repulsive nature of H_{dip} in Appendix B, the stability criterion that makes an equilibrium solution (u,v,w) for f_0 admissible, as it makes the equilibrium solution $(0,u,v,w)$ for f eligible to be the saddle point where f attains its least equilibrium value, re-

[2]See http://www.matcont.ugent.be/matcont.html.

[3]MATLAB is a registered trademark of The MathWorks, Inc. http://www.mathworks.com.

quires the Hessian matrix $\mathbb{H}$ of f at $(0,u,v,w)$ to possess two negative eigenvalues and two positive eigenvalues. To predict the possible bifurcation points along the trivial solution whence nontrivial solutions may branch off, we compute $\mathbb{H}$ at $(t,u,v,w)=(0,0,0,0)$, for varying β. An expansion of f in Eq. (37) near the origin reveals that, when expressed in the permutated variables (t,v,u,w), $\mathbb{H}$ has the following block structure

$$\mathbb{H}=\begin{bmatrix}\mathbb{H}_2 & 0\\ 0 & \mathbb{H}_2\end{bmatrix},\quad \text{with}\quad \mathbb{H}_2=\begin{bmatrix}H_{uu} & H_{uw}\\ H_{uw} & H_{ww}\end{bmatrix},$$

where

$$H_{uu}(\lambda,\alpha;\beta):=-\frac{1}{3}\cos^2\alpha\left\{4+\beta\left[\frac{16}{9}\cos^2\alpha+\left(\lambda+\frac{1}{3}\right)^2\sin^2\alpha\right]\right\},\tag{C1a}$$

$$H_{uw}(\lambda,\alpha;\beta):=-\left(\lambda+\frac{1}{3}\right)\sin\alpha\cos\alpha\left\{1+\beta\left[\frac{4}{9}\cos^2\alpha+\frac{2}{3}\left(\lambda-\frac{1}{3}\right)\sin^2\alpha\right]\right\},\tag{C1b}$$

$$H_{ww}(\lambda,\alpha;\beta):=-\sin^2\alpha\left\{2\left(\lambda-\frac{1}{3}\right)+\beta\left[\frac{4}{3}\left(\lambda-\frac{1}{3}\right)^2\sin^2\alpha+\frac{1}{3}\left(\lambda+\frac{1}{3}\right)^2\cos^2\alpha\right]\right\}.\tag{C1c}$$

It is easily seen that

$$\det\mathbb{H}_2\to-(\lambda-1)^2\cos^2\alpha\sin^2\alpha\quad\text{for}\quad\beta\to0,$$

and so in this limit, for (λ,α) in the interior $\mathring{\mathcal{P}}$ of the parameter space, $\mathbb{H}_2$ possesses one negative eigenvalue and one positive eigenvalue, which shows that, according to the criterion stated above, the trivial solution is stable at arbitrarily large temperature T. As β grows away from 0 (and T decreases), a bifurcation from the trivial solution may take place only if $\det\mathbb{H}_2$ vanishes. As is easily shown, this is the case only for

$$\beta=\beta_c(\lambda,\alpha):=\frac{3(\lambda-1)\sin^2\alpha+2+\sqrt{3(3\lambda^2-2\lambda-1)\sin^2\alpha+4}}{(\lambda-1)^2\cos^2\alpha\sin^2\alpha}.\tag{C2}$$

The analysis of the function β_c in Eq. (C2) shows that it diverges to ∞ upon approaching the following segments on $\partial\mathcal{P}$: $\{(\lambda,\alpha):\lambda\in[-1,1],\alpha=0\}$, $\{(\lambda,\alpha):\lambda=1,\alpha\in[0,\frac{\pi}{2}]\}$, and $\{(\lambda,\alpha):\lambda\in[\frac{1}{3},1],\alpha=\frac{\pi}{2}\}$, all marked by solid lines in Fig. 10. Along the segment $\{(\lambda,\alpha):\lambda\in[-1,\frac{1}{3}[,\alpha=\frac{\pi}{2}\}$, β_c tends to a finite limit, so that β_c can be extended up to there by setting

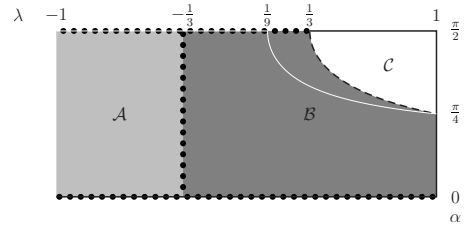

FIG. 10. The order parameter space $\mathcal{P}$ enriched with further information obtained from the bifurcation analysis of the mean-field free energy. On three segments on $\partial\mathcal{P}$, namely, $\{(\lambda,\alpha):\lambda\in[-1,1],\alpha=0\}$, $\{(\lambda,\alpha):\lambda=1,\alpha\in[0,\frac{\pi}{2}]\}$, and $\{(\lambda,\alpha):\lambda\in[\frac{1}{3},1],\alpha=\frac{\pi}{2}\}$, represented here as solid lines, the function β_c in Eq. (C2) diverges to ∞. Along the white line, which is in part on $\partial\mathcal{P}$ (for $\alpha=\frac{\pi}{2}$) and in part in $\mathcal{B}$ [for $\alpha=\alpha_0(\lambda)$ as in Eq. (C4)], β_c is stationary with respect to α. Bold points are disseminated along the locus where the function ρ in Eq. (49) vanishes. More specifically, $0<\rho<1$ in $\mathcal{A}$, $-1<\rho<0$ in $\mathcal{B}$, and $\rho<-1$ in $\mathcal{C}$.

$$\beta_c\left(\lambda,\frac{\pi}{2}\right)=\frac{9}{2}\frac{1}{1-3\lambda}.\tag{C3}$$

Moreover, along the segment $\mathcal{L}:=\{(\lambda,\alpha):\lambda\in[-1,\frac{1}{9}],\alpha=\frac{\pi}{2}\}$, $\frac{\partial\beta_c}{\partial\alpha}$ converges to zero, while it is negative at all points $(\lambda,\alpha)\in\mathring{\mathcal{P}}$ with $\lambda\in[-1,\frac{1}{9}]$. This proves that, for any given $\lambda\in[-1,\frac{1}{9}]$, the minimum of $\beta_c(\lambda,\cdot)$ falls on $\mathcal{L}$. Contrariwise, for any given $\lambda\in]\frac{1}{9},1]$, the minimum of $\beta_c(\lambda,\cdot)$ occurs in $\mathring{\mathcal{P}}$, along the curve

$$\alpha=\alpha_0(\lambda):=\arcsin\left(\frac{1}{2}\sqrt{\frac{5+3\lambda}{1+3\lambda}}\right),\quad\lambda\in\left[\frac{1}{9},1\right].\tag{C4}$$

In Fig. 10, the locus defined by Eq. (C4) is represented along with $\mathcal{L}$ as a white line. We thus conclude that the absolute minimum of β_c in $\mathcal{P}$ occurs at the vertex where $\lambda=-1$ and $\alpha=\frac{\pi}{2}$ and that

$$\min_{\mathcal{P}}\beta_c=\frac{9}{8}.\tag{C5}$$

[1] P. I. C. Teixeira, J. M. Tavares, and M. M. Telo da Gama, J. Phys.: Condens. Matter **12**, R411 (2000).
[2] J.-J. Weis and D. Levesque, Adv. Polym. Sci. **185**, 163 (2005).
[3] L. M. Blinov, Liq. Cryst. **24**, 143 (1998).
[4] M. A. Bates and G. R. Luckhurst, in *Liquid Crystals I*, edited by D. M. P. Mingos, Structure and Bonding Vol. 94 (Springer, Berlin, 1999), pp. 66–137.
[5] D. Wei and G. N. Patey, Phys. Rev. Lett. **68**, 2043 (1992).

[6] D. Wei and G. N. Patey, Phys. Rev. A **46**, 7783 (1992).
[7] D. Wei and G. N. Patey, Phys. Rev. E **47**, 2954 (1993).
[8] J. J. Weis, D. Levesque, and G. J. Zarragoicoechea, Phys. Rev. Lett. **69**, 913 (1992).
[9] J. J. Weis and D. Levesque, Phys. Rev. E **48**, 3728 (1993).
[10] D. Wei, G. N. Patey, and A. Perera, Phys. Rev. E **47**, 506 (1993).
[11] D. Wei, Phys. Rev. E **49**, 2454 (1994).
[12] J. J. Weis and D. Levesque, Phys. Rev. Lett. **71**, 2729 (1993).
[13] D. Levesque and J. J. Weis, Phys. Rev. E **49**, 5131 (1994).
[14] J. J. Weis, Mol. Phys. **93**, 361 (1998).
[15] M. E. van Leeuwen and B. Smit, Phys. Rev. Lett. **71**, 3991 (1993).
[16] B. Groh and S. Dietrich, Phys. Rev. Lett. **72**, 2422 (1994).
[17] B. Groh and S. Dietrich, Phys. Rev. E **50**, 3814 (1994).
[18] B. Groh and S. Dietrich, Phys. Rev. E **53**, 2509 (1996).
[19] M. A. Osipov, P. I. C. Teixeira, and M. M. Telo da Gama, Phys. Rev. E **54**, 2597 (1996).
[20] J. M. Tavares, M. M. Telo da Gama, and M. A. Osipov, Phys. Rev. E **56**, R6252 (1997).
[21] M. A. Osipov, P. I. C. Teixeira, and M. M. Telo da Gama, J. Phys. A **30**, 1953 (1997).
[22] P. I. C. Teixeira, M. A. Osipov, and M. M. Telo da Gama, Phys. Rev. E **57**, 1752 (1998).
[23] M. Born, Sitz. Phys. Math. **25**, 614 (1916).
[24] M. Born, Ann. Phys. **55**, 221 (1918).
[25] L. Onsager, Ann. N.Y. Acad. Sci. **51**, 627 (1949), reprinted in [59], pp. 625–657.
[26] W. Maier and A. Saupe, Z. Naturforsch. **13a**, 564 (1958), translated into English in [59], pp. 381–385.
[27] A. Perera and G. N. Patey, J. Chem. Phys. **91**, 3045 (1989).
[28] C. Vega and S. Lago, J. Chem. Phys. **100**, 6727 (1994).
[29] A. V. Emelyanenko and M. A. Osipov, Liq. Cryst. **26**, 187 (1999).
[30] A. G. Vanakaras and D. J. Photinos, Mol. Phys. **85**, 1089 (1995).
[31] M. Baus and J.-L. Colot, Phys. Rev. A **40**, 5444 (1989).
[32] B. Groh and S. Dietrich, Phys. Rev. E **55**, 2892 (1997).
[33] J. Lee and S.-D. Lee, Mol. Cryst. Liq. Cryst. **254**, 395 (1994).
[34] P. Palffy-Muhoray, M. A. Lee, and R. G. Petschek, Phys. Rev. Lett. **60**, 2303 (1988).
[35] B. Park, J. W. Wu, and H. Takezoe, Phys. Rev. E **63**, 021707 (2001).
[36] O. Kayacan, Chem. Phys. **317**, 63 (2005).
[37] F. Biscarini, C. Zannoni, C. Chiccoli, and P. Pasini, Mol. Phys. **73**, 439 (1991).
[38] F. Bisi, R. Rosso, E. G. Virga, and G. E. Durand, Phys. Rev. E **78**, 011705 (2008).
[39] R. Berardi, S. Orlandi, and C. Zannoni, Phys. Chem. Chem. Phys. **2**, 2933 (2000).
[40] M. Koike, C.-C. Yen, L. Yuqing, H. Tsuchiya, M. Tokita, S. Kawauchi, H. Takezoe, and J. Watanabe, Macromolecules **40**, 2524 (2007).
[41] A. M. Sonnet and E. G. Virga, Phys. Rev. E **77**, 031704 (2008).
[42] F. Bisi, E. G. Virga, E. C. Gartland, Jr., G. De Matteis, A. M. Sonnet, and G. E. Durand, Phys. Rev. E **73**, 051709 (2006).
[43] G. De Matteis, F. Bisi, and E. G. Virga, Continuum Mech. Thermodyn. **19**, 1 (2007).
[44] E. C. Gartland, Jr. and E. G. Virga, Arch. Ration. Mech. Anal. **196**, 143 (2010).
[45] W. H. DeJeu, Mol. Cryst. Liq. Cryst. **292**, 13 (1997).
[46] B. Groh and S. Dietrich, Phys. Rev. Lett. **79**, 749 (1997).
[47] B. Groh and S. Dietrich, Phys. Rev. E **57**, 4535 (1998).
[48] X. Zheng and P. Palffy-Muhoray, Phys. Rev. E **75**, 061709 (2007).
[49] X. Zheng, W. Iglesias, and P. Palffy-Muhoray, Phys. Rev. E **79**, 057702 (2009).
[50] A. M. Sonnet, E. G. Virga, and G. E. Durand, Phys. Rev. E **67**, 061701 (2003).
[51] J. P. Straley, Phys. Rev. A **10**, 1881 (1974).
[52] F. Bisi, S. Romano, and E. G. Virga, Phys. Rev. E **75**, 041705 (2007).
[53] F. Bisi, G. R. Luckhurst, and E. G. Virga, Phys. Rev. E **78**, 021710 (2008).
[54] B. Mettout, P. Tolédano, H. Takezoe, and J. Watanabe, Phys. Rev. E **66**, 031701 (2002).
[55] I. Fatkullin and V. Slastikov, Nonlinearity **18**, 2565 (2005).
[56] H. Zhou, H. Wang, M. G. Forest, and Q. Wang, Nonlinearity **18**, 2815 (2005).
[57] H. Liu, H. Zhang, and P. Zhang, Commun. Math. Sci. **3**, 201 (2005).
[58] M. Piastra and E. G. Virga (unpublished).
[59] T. J. Sluckin, D. A. Dunmur, and H. Stegemeyer, *Crystals that Flow* (Taylor & Francis, London, 2004).